The Life Cycle and Variability of Antarctic Weak Polar Vortex Events

XIAOCEN SHEN,[a,b] LIN WANG,[a,b] SCOTT OSPREY,[c,d] STEVEN C. HARDIMAN,[e] ADAM A. SCAIFE,[e,f] AND JI MA[a,b]

[a] *Center for Monsoon System Research, Institute of Atmospheric Physics, Chinese Academy of Sciences, Beijing, China*
[b] *College of Earth and Planetary Sciences, University of Chinese Academy of Sciences, Beijing, China*
[c] *Atmospheric, Oceanic and Planetary Physics, University of Oxford, Oxford, United Kingdom*
[d] *National Centre for Atmospheric Science, University of Oxford, Oxford, United Kingdom*
[e] *Met Office Hadley Centre, Exeter, United Kingdom*
[f] *College of Engineering, Mathematics and Physical Sciences, University of Exeter, Exeter, United Kingdom*

(Manuscript received 28 June 2021, in final form 15 December 2021)

ABSTRACT: Motivated by the strong Antarctic sudden stratospheric warming (SSW) in 2019, a survey on the similar Antarctic weak polar vortex events (WPVs) is presented, including their life cycle, dynamics, seasonality, and climatic impacts. The Antarctic WPVs have a frequency of about four events per decade, with the 2002 event being the only major SSW. They show a similar life cycle to the SSWs in the Northern Hemisphere but have a longer duration. They are primarily driven by enhanced upward-propagating wavenumber 1 in the presence of a preconditioned polar stratosphere (i.e., a weaker and more contracted Antarctic stratospheric polar vortex). Antarctic WPVs occur mainly in the austral spring. Their early occurrence is preceded by an easterly anomaly in the middle and upper equatorial stratosphere in addition to the preconditioned polar stratosphere. The Antarctic WPVs increase the ozone concentration in the polar region and are associated with an advanced seasonal transition of the stratospheric polar vortex by about one week. Their frequency doubles after 2000 and is closely related to the advanced Antarctic stratospheric final warming in recent decades. The WPV-resultant negative phase of the southern annular mode descends to the troposphere and persists for about three months, leading to persistent hemispheric-scale temperature and precipitation anomalies.

SIGNIFICANCE STATEMENT: The Antarctic weak polar vortex events (WPVs) are similar to the sudden stratospheric warming (SSW), but many of their characteristics remain unclear. Their climatology is presented as a benchmark based on high-quality reanalysis datasets. WPVs have a life cycle that is similar to that of Arctic SSWs but has a longer duration. They occur due to the amplified tropospheric wave forcing in the presence of a preconditioned polar stratosphere. Its seasonality is partly controlled by the equatorial stratospheric easterly in addition to the polar stratosphere. Its occurrence is closely related to the advanced breakdown of the Antarctic polar vortex and can reduce the size of the Antarctic ozone hole. Moreover, it further causes persistent hemispheric-scale climate anomalies in the troposphere, which provides a prediction potential for surface weather and climate.

KEYWORDS: Southern Hemisphere; Planetary waves; Stratosphere-troposphere coupling; Antarctic Oscillation; Stratospheric circulation; Quasibiennial oscillation

1. Introduction

The wintertime stratosphere is characterized by a cold polar vortex and circumpolar westerly jet, known as the polar night jet, primarily due to radiative cooling during the polar night (Andrews et al. 1987; Waugh and Polvani 2010). Sudden stratospheric warmings (SSWs) are extreme displays of polar vortex weakening and can influence both surface weather and the upper atmosphere (Andrews et al. 1987; Charlton and Polvani 2007; Butler et al. 2015; Baldwin et al. 2021). They are characterized by sharp rises of temperature in the polar stratosphere and strong deceleration of the polar night jet (Andrews et al. 1987). Due to these dramatic circulation changes, SSWs can significantly alter the composition and dynamics of the stratosphere and also influence the mesosphere, thermosphere, and ionosphere (Eswaraiah et al. 2017; Pedatella et al. 2018; Baldwin et al. 2021). Moreover, the SSW-associated circulation anomalies sometimes descend into the troposphere and exert remarkable impacts on tropospheric weather conditions (Baldwin and Dunkerton 1999, 2001; Kolstad et al. 2010; Kidston et al. 2015) and prediction skills on subseasonal to seasonal time scales (Scaife et al. 2016; Domeisen et al. 2020).

SSWs can be observed in both hemispheres, but their frequency and intensity show significant interhemispheric asymmetry, with fewer events in the Southern Hemisphere. SSWs can be termed *minor warming* if the stratospheric (e.g., at 10 hPa) temperature gradient between polar and midlatitudes reverses alone, and *major warming* if the polar night jet further reverses to easterly (Andrews et al. 1987; Butler et al. 2015). *Major* SSWs usually occur in the Northern Hemisphere, where six events are observed per decade on average (Charlton and Polvani 2007). In contrast, only one *major* SSW was observed so far in the Southern Hemisphere in 2002 (Charlton et al. 2005; Manney et al. 2005; Newman and Nash 2005), and it is estimated to occur only once every 25 years or so (Wang et al. 2020; Jucker et al. 2021). This contrast in frequency is primarily attributed to the weaker wave forcing

Corresponding author: Lin Wang, wanglin@mail.iap.ac.cn

DOI: 10.1175/JCLI-D-21-0500.1

induced by weaker land–sea thermal contrasts and smaller orography in the Southern Hemisphere (Plumb 1989; Scaife and James 2000; Waugh and Polvani 2010). Nevertheless, *minor* SSWs associated with extreme weakening of the polar vortex still occur in the Southern Hemisphere (Hirota et al. 1990; Kanzawa and Kawaguchi 1990; Lim et al. 2018). For example, the *minor* SSW in September 2019 was accompanied by the most elevated stratospheric polar warming and the smallest ozone hole on record (Rao et al. 2020a; Safieddine et al. 2020; Shen et al. 2020a; Wargan et al. 2020; Lim et al. 2021). This fact indicates that *minor* SSWs in the Southern Hemisphere still warrant thorough understanding because of their climatic influences.

Some case studies documented the characteristics of certain Antarctic SSW events (e.g., Hirota et al. 1990; Newman and Nash 2005; Lim et al. 2021) and compared them with those in the Northern Hemisphere, including the persistence of tropospheric blocking, the phase of stratospheric equatorial wind, and the influences of the SSWs on the tropospheric circulation and weather (e.g., Nishii and Nakamura 2004; Gray et al. 2005; Rao et al. 2020a; Shen et al. 2020a,b). However, there is no systematic analysis of the climatological characteristics of the Antarctic SSWs to the best of the authors' knowledge. Therefore, this study tries to fill this knowledge gap by revealing the Antarctic SSW's life cycle, dynamics, seasonality, and impacts on both the stratosphere and troposphere from a climatological point of view. It is noteworthy that there are only two consensus Antarctic SSW events, the 2002 and 2019 cases (Baldwin et al. 2021), before the publication of this study and that the academic community is cautious about using the term SSW in the Southern Hemisphere. Therefore, we refer to the events investigated in this study as weak polar vortex events (WPVs). Compared with previous studies that address the tropospheric response to the negative stratospheric southern annular mode (e.g., Thompson et al. 2005; Kwon et al. 2020), this study focuses on the characteristics and dynamics of the WPVs. The paper is organized as follows. Section 2 describes the datasets used in the study and the definition of Antarctic WPVs. Section 3 presents the life cycle and dynamics of the Antarctic WPVs. Section 4 investigates the seasonality and possible causes of the Antarctic WPVs. Section 5 shows the impacts of the Antarctic WPVs on the stratosphere and the troposphere. Finally, section 6 summarizes the main findings.

2. Data and method

a. Data

The daily mean atmospheric reanalysis data used in this study are from several sources, including the Japanese 55-year Reanalysis dataset (JRA-55; Kobayashi et al. 2015), the latest European Centre for Medium-Range Weather Forecasts dataset (ERA5; Hersbach et al. 2020), the ERA-Interim dataset (Dee et al. 2011), and the National Centers for Environmental Prediction–National Center for Atmospheric Research (NCEP–NCAR) reanalysis dataset (Kalnay et al. 1996). The hourly total column ozone data is adopted from the second Modern-Era Retrospective analysis for Research and Applications (MERRA-2) reanalysis dataset (Gelaro et al. 2017) and averaged into daily means. It is used to present the horizontal structure of ozone anomalies associated with the WPVs. The daily polar-cap ozone data (south of 63°S) are from the National Aeronautics and Space Administration (NASA) Ozone Watch (https://ozonewatch.gsfc.nasa.gov) and used to show the statistical distribution of polar-cap ozone after the onset of WPVs. The precipitation data are from the Climate Prediction Center (CPC) Global Unified Precipitation dataset produced by National Oceanic and Atmospheric Administration (NOAA) (Xie et al. 2007; Chen et al. 2008). Due to the limited observations at high latitudes of the Southern Hemisphere before 1979 and the satellite observing era, this study focuses on the 1979–2019 period. A daily climatology is defined as the value averaged over 1979–2019 (except for the total column ozone, which is over 1980–2019) for each calendar day, and the daily anomaly is defined as the departure from this daily climatology.

b. Definition of WPV

The SSWs are usually defined based on the reversal of the stratospheric pole-to-midlatitude temperature gradient or the stratospheric circumpolar zonal-mean zonal wind (e.g., Andrews et al. 1987; Butler et al. 2015). This study follows the definition of *minor* SSWs (Andrews et al. 1987) and defines an Antarctic WPV when the temperature gradient between the South Pole and midlatitudes reverses in the stratosphere. Specifically, the poleward temperature gradient (∇T) is defined as the zonal-mean temperature averaged from 80° to 90°S minus that averaged from 60° to 70°S at 10 hPa. This approach is similar to that used by Butler et al. (2015), which focuses on the SSWs in the Northern Hemisphere. With this definition, a positive poleward ∇T indicates a warmer polar region. An Antarctic WPV is identified when the following three criteria are met:

- the reversal of the poleward ∇T at 10 hPa lasts for at least 5 days with the maximum value exceeding the climatological value by one standard deviation on the corresponding calendar day;
- the averaged temperature anomaly southward of 60°S at 10 hPa is positive;
- two WPVs in the same season are separated by at least a 60-day period.

The threshold values in the first criterion were tested, ranging from 0.5 to 1.5 standard deviations, respectively, and the results show little sensitivity (not shown). The duration parameter in the first criterion was based on the composite evolution of all identified abnormal temperature gradient reversal events with a 1.0 standard deviation. It was also tested from 2 to 10 days, and the results remain similar (not shown). Reversals of temperature gradients can be caused by warming in the polar region and/or cooling in the midlatitudes. Hence, the second criterion was included to constrain that the identified events are weak polar vortex events with rising polar temperatures. The first day that the poleward ∇T reverses in the above definition is regarded as day 0 of the

TABLE 1. WPVs in JRA-55, ERA5, ERA-Interim, and NCEP–NCAR datasets. The unit of frequency is events per year.

Event no.	JRA-55	ERA5	ERA-Interim	NCEP–NCAR
1	1 Oct 1979	1 Oct 1979	2 Oct 1979	23 Aug 1979
2	—	—	18 Oct 1982	19 Oct 1982
3	6 Oct 1984	5 Oct 1984	—	—
4	26 Sep 1988	26 Sep 1988	27 Sep 1988	26 Sep 1988
5	20 Oct 1989	20 Oct 1989	—	—
6	30 Sep 1992	30 Sep 1992	30 Sep 1992	30 Sep 1992
7	1 Oct 2000	1 Oct 2000	9 Oct 2000	1 Oct 2000
8	21 Sep 2002	21 Sep 2002	21 Sep 2002	21 Sep 2002
9	11 Oct 2003	11 Oct 2003	5 Oct 2003	11 Oct 2003
10	6 Oct 2005	2 Oct 2005	6 Oct 2005	6 Oct 2005
11	3 Oct 2007	18 Sep 2007	18 Sep 2007	3 Oct 2007
12	—	13 Oct 2008	13 Oct 2008	—
13	8 Oct 2009	8 Oct 2009	8 Oct 2009	8 Oct 2009
14	4 Oct 2012	30 Sep 2012	30 Sep 2012	4 Oct 2012
15	2 Oct 2013	30 Sep 2013	30 Sep 2013	2 Oct 2013
16	—	—	5 Oct 2014	9 Oct 2014
17	—	—	3 Oct 2016	—
18	19 Sep 2017	12 Sep 2017	12 Sep 2017	19 Sep 2017
19	6 Sep 2019	6 Sep 2019	—	6 Sep 2019
Total No. of events	15	16	16	15
Frequency	0.37	0.39	0.40	0.37

WPVs. Moreover, to distinguish the WPVs from the seasonal breakdown of the stratospheric polar vortex, the occurrence dates (day 0) of WPVs should be at least 20 days before the stratospheric final warming (SFW). The SFW in the Southern Hemisphere was defined as the final date when the 5-day running mean zonal-mean zonal wind at 60°S ($[u_{60}]$) at 50 hPa drops below 10 m s^{-1} (Black and McDaniel 2007) in each winter. Considering the earlier occurrence of the SFW signal in the upper than in the lower stratosphere (Hardiman et al. 2011; Byrne and Shepherd 2018; Lim et al. 2018, 2019), the $[u_{60}]$ at 10 hPa is used in this study to replace the $[u_{60}]$ at 50 hPa in the original definition to be comparable to the definition of WPVs. The identified SFWs are, on average, one month behind the occurrence of WPVs. In addition, the breakdown of the stratospheric polar night jet is another 12 days behind, when the zonal wind completely switches to the easterly (Table 1, Figs. 3c and 11). This result suggests that the WPV and SFW in the Southern Hemisphere are distinguishable, although their time lag is not as large as that of their Northern Hemispheric counterparts (Hu et al. 2014).

c. Southern annular mode

The southern annular mode (SAM) is defined as the leading empirical orthogonal function of the seasonal (September–December) mean geopotential height anomalies south of 20°S at each of the 37 pressure levels during 1979–2019, where the seasonal mean is calculated from the monthly mean data (Thompson et al. 2005). The daily SAM index is obtained by projecting the daily geopotential height anomalies onto the respective patterns of the SAM at each pressure level. Note that with this approach, the seasonal evolution is excluded, and the EOF patterns mainly reflect the change in the strength of the polar vortex. This approach differs from the height–time domain EOF method in Lim et al. (2018), which captures the seasonal breakdown of the vortex.

d. Bootstrap technique

The bootstrap technique is used to estimate the probability density functions (PDFs) of a finite sample (Efron and Tibshirani 1994). For a group with the sample size n, we apply the sampling with replacement to obtain a new group with the same sample size n. This process is repeated 1000 times to yield 1000 new groups. Then the PDF of the original finite sample is obtained based on the mean of each new group.

3. Life cycle and dynamics of the Antarctic WPVs

The occurrence of a WPV indicates dramatic changes in the stratospheric polar vortex, so it is meaningful to first look at the stationarity of the stratospheric polar vortex from the climatological perspective. Figure 1 shows the daily evolution of climatology (contours) and the interannual standard deviation (shading) of $[u_{60}]$ and the poleward ∇T at 10 hPa in different datasets. The standard deviation is normalized by dividing the mean value of the corresponding layer to reconcile the magnitudes of variability at different pressure levels. The Antarctic stratospheric polar vortex reaches its highest intensity in early August and has the strongest variance from late August to November, first in the upper stratosphere and then in the lower levels (Fig. 1, left column). It also has a second and weaker peak of $[u_{60}]$ variance in the upper stratosphere in midwinter, consistent with Waugh and Randel (1999). From late winter to spring, the Antarctic stratospheric polar vortex has the largest variability and facilitates the occurrence of the WPVs. This seasonality can be explained by the enhanced planetary wave forcing originating from the troposphere when the background stratospheric westerly wind begins to weaken and allows the

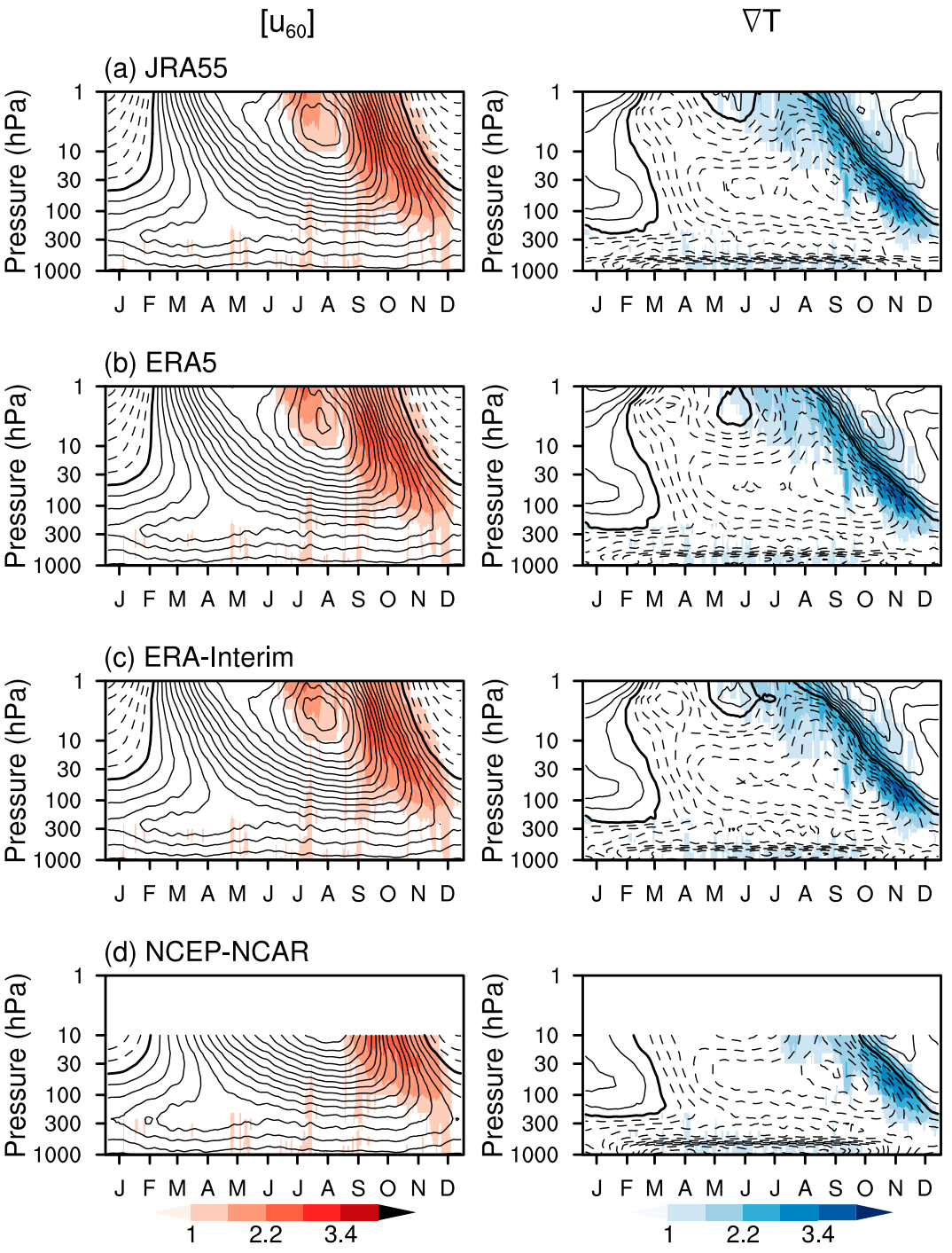

FIG. 1. (left) Daily evolution of the climatology [contours; contour interval (CI) = 5 m s^{-1}] and the scaled interannual standard deviation [shading; shading interval (SI) = 0.6] of zonal-mean zonal wind at 60°S ([u_{60}]) in the (a) JRA-55, (b) ERA5, (c) ERA-Interim, and (d) NCEP–NCAR reanalysis datasets. Negative values are dashed, with the zero contours in bold. (right) As in the left column, but for the poleward temperature gradient (∇T) between 80°–90°S and 60°–70°S (CI = 2 K, SI = 0.6).

vertical propagation of large-scale Rossby waves (Charney and Drazin 1961). Before this time, the stratospheric westerly wind is so strong that even the longest vertically propagating Rossby waves are often reflected back to the troposphere (Scaife and James 2000; Shaw et al. 2011). The above evolving characteristics, which are highly consistent in all the four datasets, are also visible in ∇T (Fig. 1, right column) and similar to those revealed by the SAM index (Thompson et al. 2005).

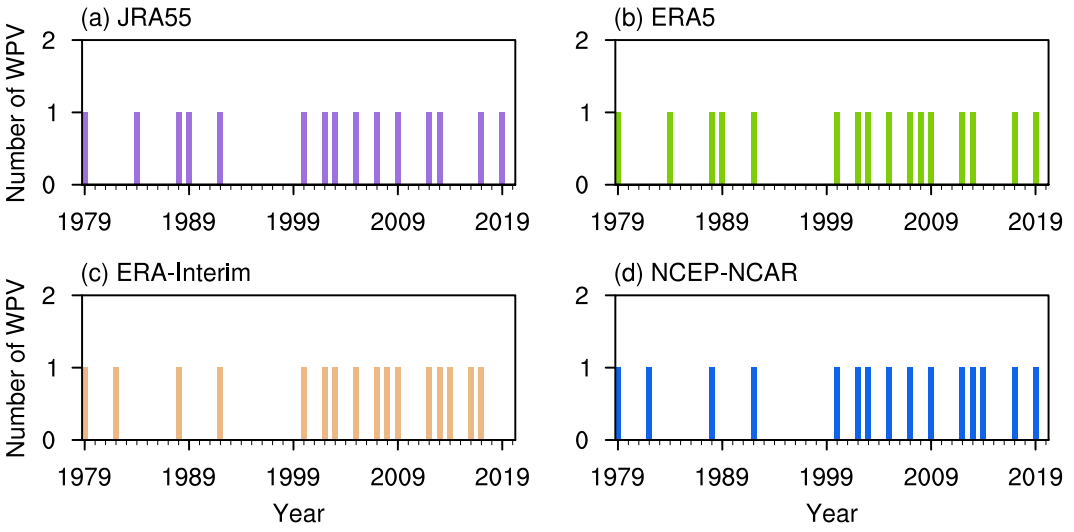

FIG. 2. The number of Antarctic WPVs by year in the (a) JRA-55, (b) ERA5, (c) ERA-Interim, and (d) NCEP–NCAR datasets.

Table 1 shows the identified Antarctic WPVs and their central dates (day 0) in the four datasets. The numbers and central dates of the WPVs are highly consistent in these reanalysis products. Fifteen WPVs are identified in the JRA-55 and NCEP–NCAR reanalysis datasets with a frequency of 0.37 per year, and 16 WPVs are identified in the ERA5 and ERA-Interim reanalysis datasets with a frequency of 0.39 and 0.40 per year, respectively. The frequency remains similar if data prior to 1979 are included. The 2002 *major* SSWs (e.g., Manney et al. 2005; Scaife et al. 2005) and 2019 *minor* SSWs (e.g., Rao et al. 2020a; Shen et al. 2020a; Lim et al. 2021) are both identified in all datasets except in the ERA-Interim dataset, which terminated in August 2019. The yearly distribution of WPVs suggests that more frequent WPVs are observed after 2000 (about 0.5 events per year) than before 2000 (about 0.25 events per year) in all the four datasets (Fig. 2). This increasing trend in frequency is consistent with Kwon et al. (2020), who analyzed the trend of the SAM, and is insensitive to the parameters in the definition of WPVs. The reason for this increasing trend may be the recovery of ozone since 2000, which can weaken the stratospheric polar vortex by enhancing the absorption of radiation (Jucker et al. 2014; Solomon et al. 2016), and the changes in the large-scale tropospheric circulation around 2000 (e.g., Hu and Fu 2009; Yeh et al. 2009; Trenberth and Fasullo 2013). This trend may also be attributed to the absence of WPVs in the 1990s. A similar gap also occurs in the Northern Hemisphere, where only two SSWs were observed in the 1990s (Butler et al. 2015; Domeisen 2019; Baldwin et al. 2021). It indicates the necessity to systematically study the causes of the frequency change in the Antarctic WPVs and compare it with the Northern Hemisphere. In the following paragraphs, the life cycle of the Antarctic WPVs will be presented. Results obtained in all four datasets are almost identical, so only those based on the JRA-55 reanalysis dataset are shown.

Figure 3 illustrates the composited day-to-day evolution of several variables during the Antarctic WPVs. Before day 0, the 10-hPa ∇T is negative, and the polar night jet is stronger than 50 m s^{-1} (Fig. 3a), indicating a stable stratospheric polar vortex. From day −2 to day +1, where minus and plus indicate days before and after day 0, the polar night jet decelerates to below 30 m s^{-1}. Meanwhile, the 10-hPa ∇T reverses with higher temperature over the polar region than the midlatitudes, marking the occurrence of the WPV. Figure 3b further shows the anomalies of $[u_{60}]$ and ∇T after removing the annual cycle to highlight the changes during the WPV. The deceleration of the polar night jet and the weakening of the poleward temperature gradient become visible approximately two weeks before day 0. They intensify abruptly from day −2 to day +2 and persist significantly for about one month (Fig. 3b). This persistent zonal wind anomaly may be associated with an advanced seasonal breakdown of the polar vortex, which will be further discussed in section 5. In this process, the anomalies of ∇T, $[u_{60}]$, and polar-cap (60°–90°S) temperature (T_{cap}) first appear in the middle and upper stratosphere and then in the lower stratosphere and upper troposphere (Figs. 3d–f). On some occasions, anomalies can also be found in the middle troposphere (Figs. 3d–f). The overall descending processes persist for nearly three months, which are more long-lasting than their counterparts in the Northern Hemisphere (Baldwin et al. 2003; Limpasuvan et al. 2004; Thompson et al. 2005).

Following Limpasuvan et al. (2004), we divide the life cycle of WPV into six stages, the onset (from days −32 to −20), growth (from days −19 to −7), mature (from days −6 to +6), descending (from days +7 to +19), decline (from days +20 to +32), and decay (from days +33 to +45) stages. Figure 4 shows the anomalies of geopotential height and temperature at 10 hPa during different stages. A wavenumber-1 height pattern is visible during the onset stage with an anomalous anticyclone over the Southern Ocean to the southeast of Australia (Fig. 4a). This pattern persists and intensifies in the growth and mature stages (Figs. 4a–c), becomes zonally symmetric, occupies the polar region from the mature stage

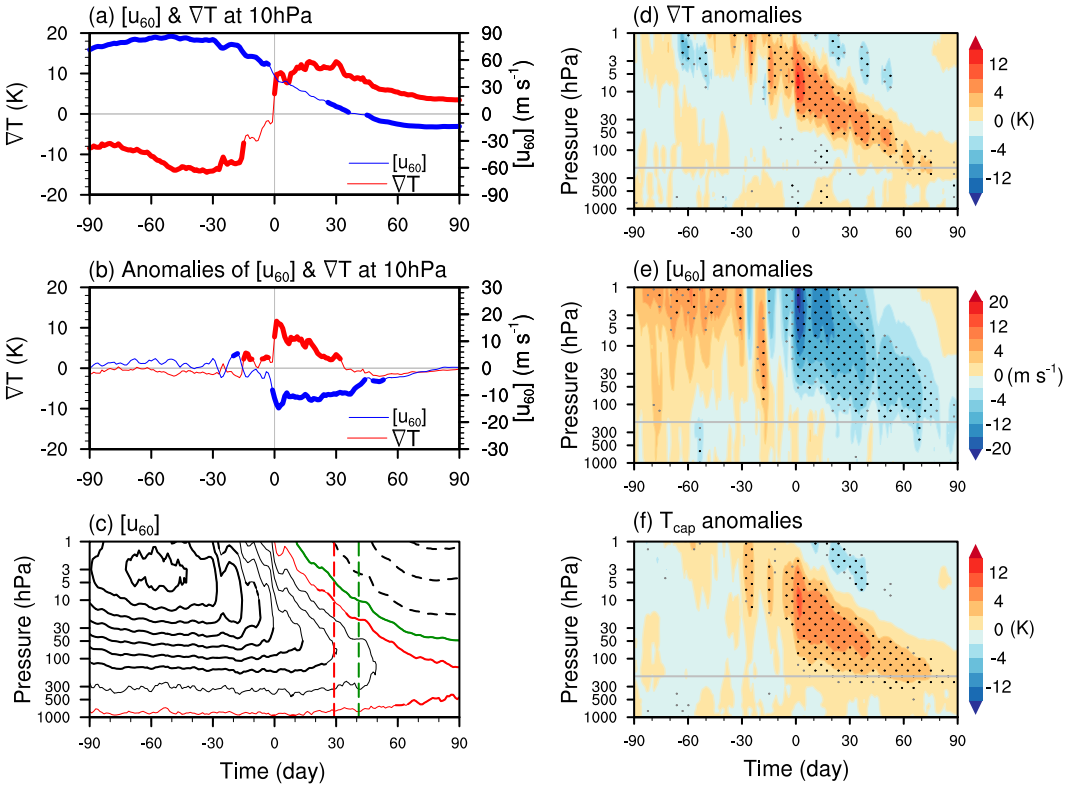

FIG. 3. (a) Daily evolution of the $[u_{60}]$ (blue line) and ∇T (red line) at 10 hPa during the composite life cycle of Antarctic WPVs. (b) As in (a), but for anomalies of $[u_{60}]$ and ∇T. (c) As in (a), but for all levels from 1000 to 1 hPa. Daily evolution of (d) ∇T anomalies (shading; ±2, ±4, ±8, ±12, ±16; K), (e) $[u_{60}]$ anomalies (±2, ±4, ±8, ±12, ±16, ±20; m s^{-1}), and (f) T_{cap} anomalies (±2, ±4, ±8, ±12, ±16; K) during the composite life cycle of Antarctic WPVs. Thick lines in (a)–(c) and black (gray) dots in (d)–(f) indicate values exceeding the 95% (90%) confidence level based on the two-tailed Student's t test. Red and green contours in (c) denote 10 and 0 m s^{-1}, respectively. The red and green vertical dashed lines in (c) show the date when the $[u_{60}]$ at 10 hPa drops below 10 and 0 m s^{-1}, respectively. The gray horizontal line in (d)–(f) indicates the approximate boundary between the troposphere and the stratosphere.

onward, and weakens from the descending to decay stages (Figs. 4c–f). The location and intensity of the observed polar warming, which is caused by anomalous downwelling in the residual circulation, generally follow those of the anomalous anticyclone. Besides, a zonally symmetric cooling is visible in the low latitudes during the mature and descending stages (Figs. 4c,d), which arises from the associated strengthening of the rising branch of the residual circulation and the resultant adiabatic cooling (Matsuno 1971; Andrews et al. 1987). The wavy structure prior to the mature stage suggests the essential role of the planetary-scale Rossby waves in forming the WPV. Meanwhile, the geographic preference of the wave structure is likely related to the zonally asymmetric topography of the Southern Hemisphere and the zonally asymmetric deep atmospheric convection in the tropics (Mechoso et al. 1988; Charlton et al. 2005; Garfinkel et al. 2013; Goyal et al. 2021).

To further reveal the essential role of the Rossby waves in the Antarctic WPVs, Fig. 5 shows the stage-averaged anomalies of zonal-mean zonal wind, zonal-mean temperature, and Eliassen–Palm (EP) flux and its divergence. During the onset stage, there are westerly and easterly anomalies above 50 hPa to the south and north of 60°S, respectively (first column in Fig. 5a). This configuration indicates that the stratospheric polar vortex contracts poleward prior to the occurrence of WPVs, as the core of the polar night jet is located at 60°S (not shown). It yields positive refractive index anomalies at the edge of the polar vortex, thus setting a favorable precondition for effective upward propagation and focusing of quasi-stationary Rossby waves toward the stratospheric polar vortex (not shown; McIntyre 1982; Andrews et al. 1987). As a result, the upward-propagating EP flux into the stratosphere increases and leads to enhanced EP flux convergence around 60°S in the upper stratosphere (first column in Fig. 5b) and deceleration of the polar night jet during the growth stage (second column in Fig. 5a). The upward-propagating EP flux continues to amplify between 50° and 80°S in the middle and upper stratosphere from the growth to mature stages (second and third columns in Fig. 5b), leading to intensified EP flux convergence and deceleration of the polar night jet (third and fourth columns in Fig. 5a). This upward propagation gradually weakens during the descending stage (fourth column in Fig. 5b) and shows an anomalous downward propagation from decline to decay

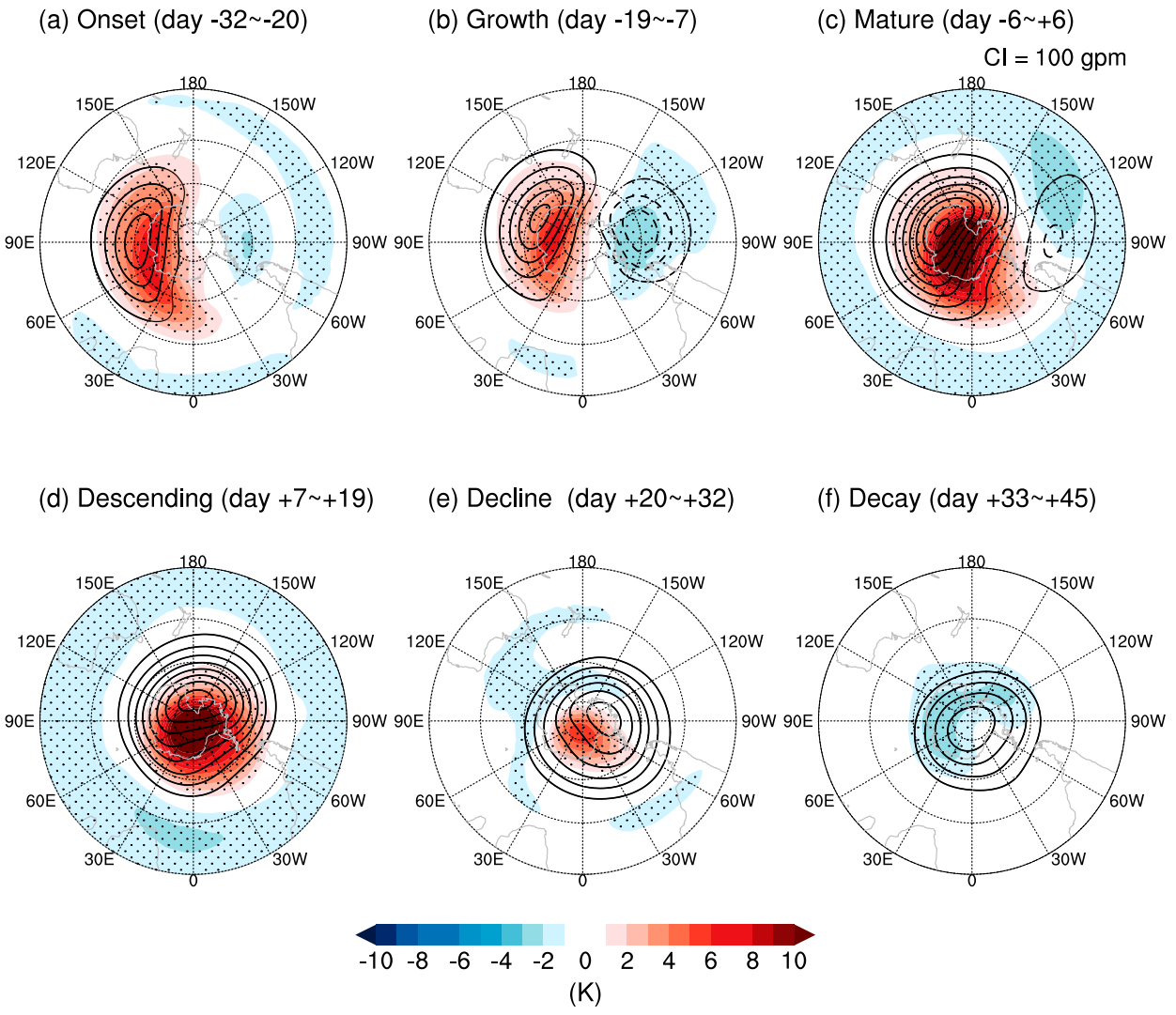

FIG. 4. Anomalies of temperature (shading; SI = 1 K) and geopotential height (contours; CI = 100 gpm) at 10 hPa during different stages of the composite life cycle of Antarctic WPVs. Zero contours are omitted, and negative contours are dashed. Black dots indicate temperature anomalies exceeding the 95% confidence level based on the two-tailed Student's *t* test.

stages (fifth and sixth columns in Fig. 5b). Accordingly, the EP flux convergence to the south of approximately 50°S weakens and descends from the upper to the lower stratosphere (fourth to sixth columns in Fig. 5b). As a result, the easterly anomalies of the polar night jet weaken and descend to the lower stratosphere and even to the troposphere, forming the negative SAM-like structure in the troposphere (fourth to sixth columns in Fig. 5a).

It is worth mentioning that enhanced poleward propagation of EP flux is also evident in the extratropical troposphere besides the weakened upward EP flux toward the stratosphere during the descending and decline stages (fourth and fifth columns in Fig. 5b). The meridional EP flux has an opposite sign to the eddy momentum flux (Andrews et al. 1987), so this configuration denotes an enhanced equatorward eddy momentum flux, which plays a crucial role in transmitting the stratospheric anomalies to the troposphere (Limpasuvan et al. 2004; Kidston et al. 2015). The EP flux anomalies during the decline and decay stages of the WPV are roughly opposite to those during the onset and growth stages (Fig. 5b), presumably due to the "shielding" by the reduced winds at lower levels. In response to the anomalous wave propagation and the associated circulation change, robust warming first appears in the upper stratosphere during the onset and growth stages (first and second columns in Fig. 5c). It descends and peaks in the middle stratosphere during the mature stage (third column in Fig. 5c) and further descends to the lower stratosphere and upper troposphere from the descending to decay stages (fourth to sixth columns in Fig. 5c).

The above evolutions of dynamical and thermal variables are overall similar to those of the SSWs in the Northern Hemisphere (Limpasuvan et al. 2004), including the

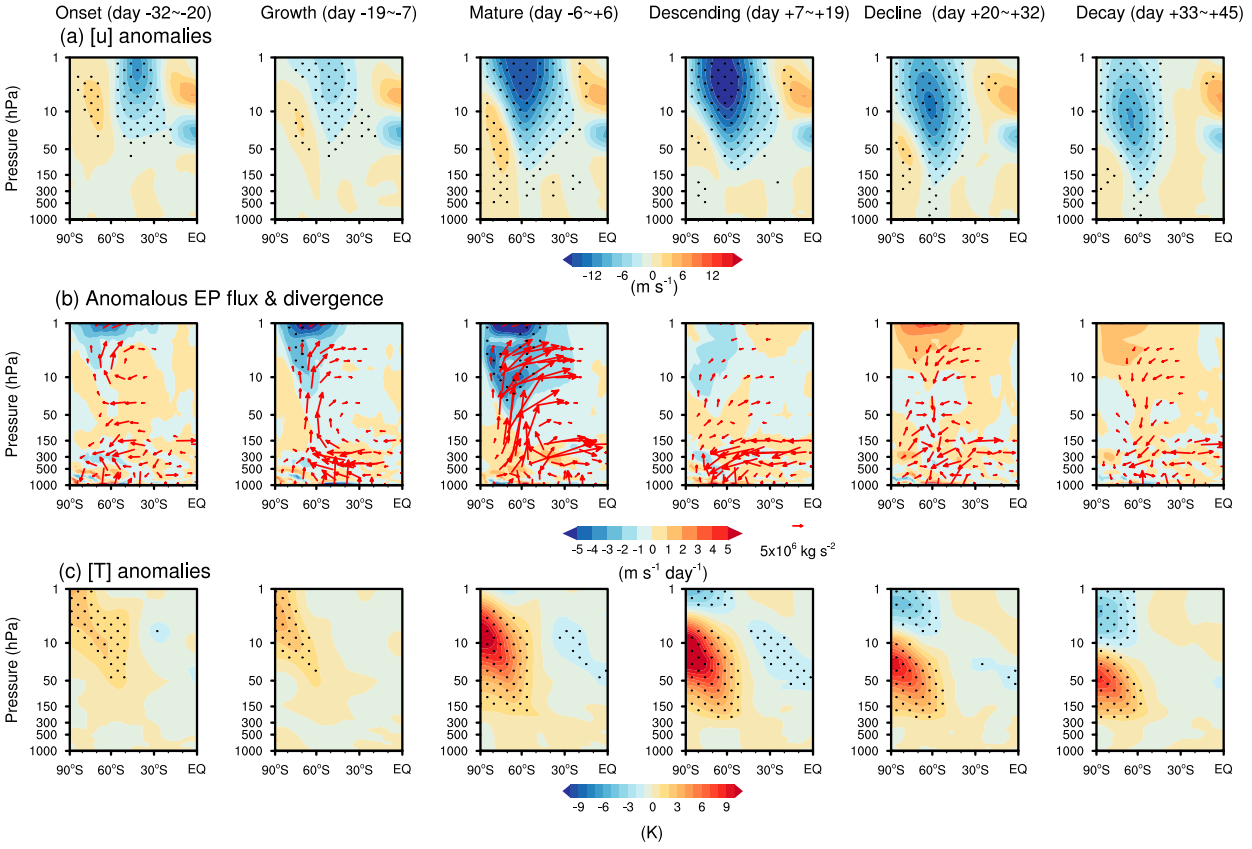

FIG. 5. Anomalies of (a) zonal-mean zonal wind (SI = 2 m s^{-1}), (b) EP flux (vector; kg s^{-2}) and its divergence (shading; SI = 1 m s^{-1} day^{-1}), and (c) zonal-mean temperature (SI = 1 K) during different stages of the composite life cycle of Antarctic WPVs as in Fig. 4. Black dots indicate shading exceeding the 95% confidence level based on the two-tailed Student's *t* test. Columns from left to right denote the onset, growth, mature, descending, decline, and decay stages, respectively.

behavior of the quasi-stationary Rossby waves, the deceleration of the polar night jet, and the warming in the polar region. In addition, the stratospheric equatorial wind during the Antarctic WPVs shows easterly and westerly anomalies centered at 30 and 5 hPa (Fig. 5a), respectively, resembling the quasi-biennial oscillation (QBO; e.g., Baldwin et al. 2001) signature during the Arctic SSWs (Limpasuvan et al. 2004) despite with lower statistical significance. This wind signature can be traced back to several months earlier (not shown), highlighting the potential importance of preconditioning for Southern Hemisphere WPV events (Scaife et al. 2005; Lim et al. 2021). Nevertheless, this wind configuration is missing and even reversed in the two SSWs in 2002 and 2019 (Gray et al. 2005; Shen et al. 2020b), which will be further discussed in section 4.

Figure 6 shows the day-to-day evolution of the anomalous EP flux components over the high latitudes (poleward of 50°S) to further delineate the wave forcing during the life cycle of Antarctic WPVs. The anomalies have been normalized by dividing by the climatological standard deviation at each level, which allows easy comparison of the wave bursts with general variability at that level (Jucker 2016; White et al. 2019). Above-normal upward EP fluxes (Fz) start to emerge in the stratosphere on approximately day −40 and persist to day +10 (Fig. 6a). During this process, a significant intensification of Fz occurs around day −10, indicating a Rossby wave pulse into the stratosphere before the occurrence of the WPV. This abnormal wave pulse mainly originates from the upward-propagating tropospheric waves of wavenumber 1 (Fig. 6b), which is partly offset by wavenumbers 2 and 3 (Figs. 6a,c,d). Previous studies suggest that the persistence and accumulation of Rossby wave activity play a more important role in decelerating the polar night jet than the wave activity pulse strength (Polvani and Waugh 2004; Sjoberg and Birner 2012). However, the strong and significant Fz originated from the troposphere prior to day 0 suggests that the Rossby wave pulses also contribute essentially to the occurrence of Antarctic WPVs (Fig. 6b). The Rossby wave propagates equatorward (Fig. 6e; Fy, positive value) after entering the stratosphere, consistent with the results shown in Fig. 5b. An inspection of individual wave components suggests that wavenumber 1 dominates the upward and equatorward wave propagation in the stratosphere (Fig. 6), which is similar to the situation in the Northern Hemisphere (Limpasuvan et al. 2004). This result agrees with the wavenumber-1 pattern in the geopotential height field (Fig. 4) and the theory that only large-scale

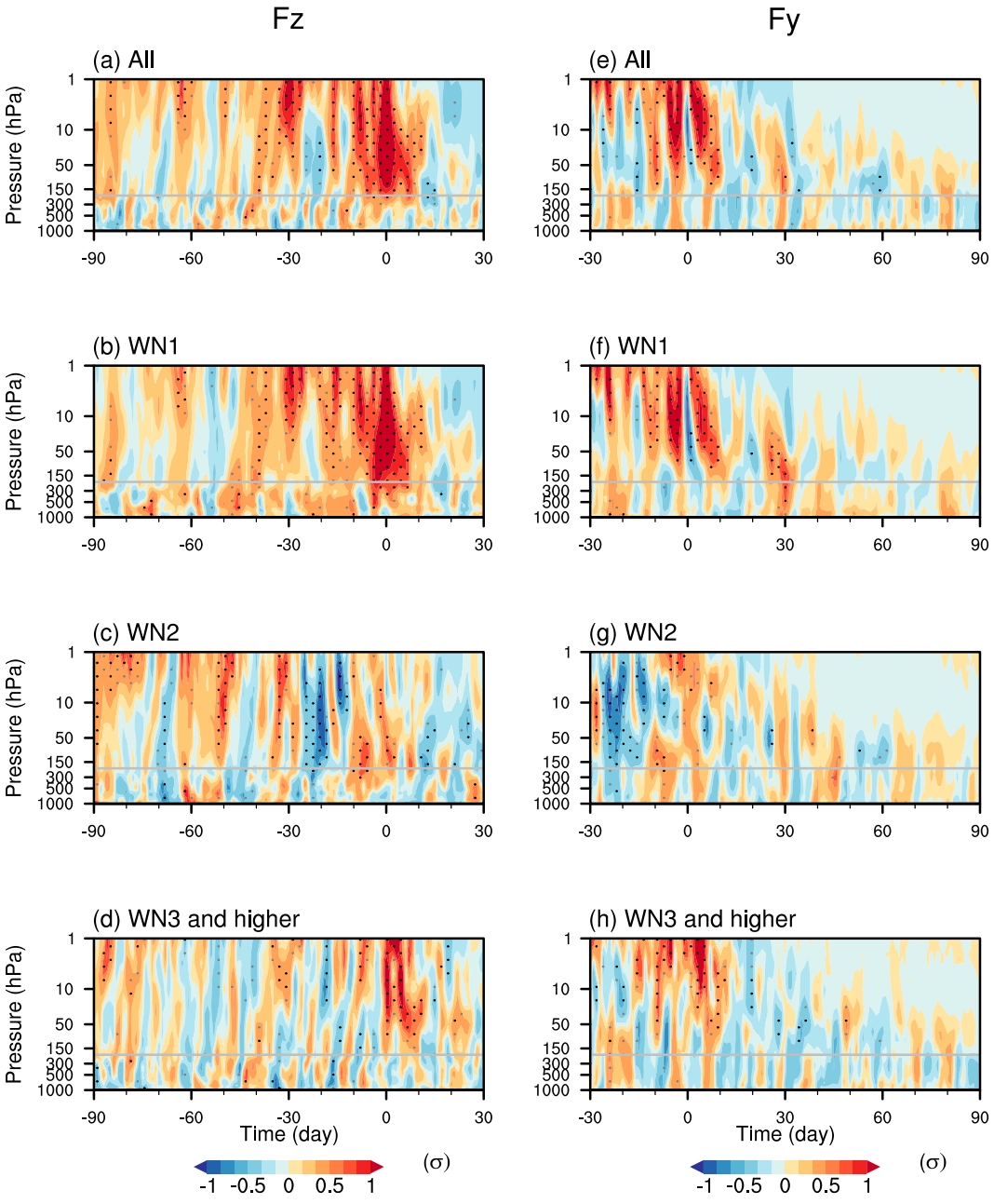

FIG. 6. The daily evolution of the vertical component of the EP flux (Fz) anomalies (shading; ±0.1, ±0.25, ±0.5, ±0.6, ±0.8, ±1.0; σ) averaged poleward of 50°S for (a) all wavenumbers, (b) wavenumber 1, (c) wavenumber 2, and (d) wavenumber 3 and higher during the composite life cycle of Antarctic WPVs. (e)–(h) As in (a)–(d), but for the horizontal component of the EP flux (Fy) anomalies. Both Fz and Fy have been scaled by the climatological standard deviation at each level so that the shadings have no unit. Black and gray dots indicate values exceeding the 95% and 90% confidence level based on the two-tailed Student's t test, respectively. The gray horizontal line indicates the approximate boundary between the troposphere and the stratosphere.

waves can propagate through strong westerlies into the stratosphere (Charney and Drazin 1961).

After day 0, anomalous poleward propagation of Rossby wave (negative Fy) is visible in the troposphere (Fig. 6e), which persists for about three months. The persistence characteristics of Fy are somewhat noisy, so a bootstrap technique is applied to test the robustness of the signal further. Figure 7 shows the PDFs of the 500-hPa Fy anomalies averaged poleward of 50°S and from day 0 to day +90 estimated from 1000 bootstrap samples. The 95th percentile of Fy for all wavenumbers is negative (black dashed line), and this result is insensitive to the specified tropospheric level. It indicates that the

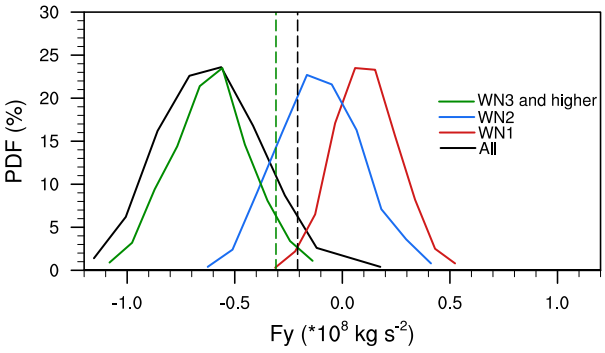

FIG. 7. PDF (solid curve) of the 500-hPa Fy anomalies averaged poleward of 50°S and from day 0 to day +90 estimated from 1000 bootstrap samples. The solid black, red, blue, and green curves indicate Fy for all wavenumbers, WN1, WN2, and WN3 and higher, respectively. The black and green vertical dashed lines indicate the 95th percentiles for all wavenumbers and WN3 and higher, respectively.

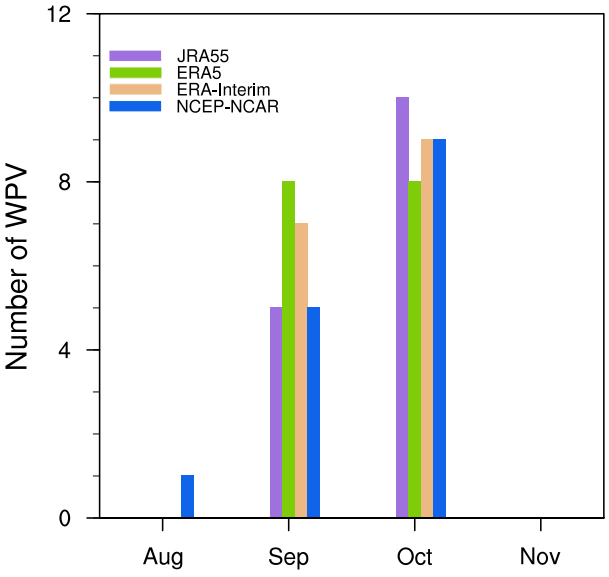

FIG. 8. Distribution of the number of Antarctic WPVs by month in the four reanalysis datasets. Purple, green, brown, and blue indicate results derived from the JRA-55, ERA5, ERA-Interim, and NCEP–NCAR datasets, respectively.

anomalous poleward propagation of Rossby waves plays a dominant role in the troposphere. Moreover, the anomalous poleward propagation is dominated by wavenumber 3 and higher (Figs. 6h and 7), indicating that smaller-scale waves are responsible for the tropospheric responses to the descending Antarctic WPV signals. Despite the lower statistical significance and relatively noisy signal, the above processes are similar to the SSWs in the Northern Hemisphere (Limpasuvan et al. 2004). The weaker and less significant signals are possibly due to the rareness of *major* SSW in the Southern Hemisphere and the relatively less significant descending of the stratospheric signal into the lower troposphere (Figs. 3d–f). Nevertheless, the results' high similarity suggests that the downward stratosphere–troposphere coupling dynamics following WPVs are fairly similar in both hemispheres.

4. Seasonality of the Antarctic WPVs

Figure 8 shows the total number of WPV events in each month in all four datasets. The number is the highest in October and then September, and only one occurs in August, according to the NCEP–NCAR data. This result suggests that most Antarctic WPVs occur in early austral spring. This is in sharp contrast to the Arctic SSWs with a relatively homogeneous distribution among months, albeit with more occurring during mid- and late winter (Charlton and Polvani 2007; Horan and Reichler 2017; Rao et al. 2021a). Therefore, Antarctic WPVs are more strongly related to the seasonal cycle than Arctic SSWs. This is because the stratospheric polar vortex in the Southern Hemisphere is stronger and more stable than in the Northern Hemisphere (Hio and Yoden 2005; Waugh and Polvani 2010; Byrne and Shepherd 2018). The wave–mean flow interactions cannot dramatically alter the Antarctic stratospheric polar vortex until austral spring when the vortex diminishes in strength (Baldwin et al. 2003).

It is inferred that the Antarctic WPVs occurring earlier need stronger Rossby wave forcing from the troposphere than those occurring late. Figure 9a shows the scatterplot of the WPV timing (x axis) versus the Rossby wave activity entering the stratosphere before the WPV, represented by the eddy heat flux anomalies averaged between 45° and 75°S at 100 hPa from day −40 to day 0 (y axis). Here, the variables in Fig. 9 are daily anomalies calculated by removing the seasonal cycle. As such, greater absolute values of y-axis variables denote the larger deviation values. The negative eddy heat flux indicates the upward propagation of Rossby waves in the Southern Hemisphere (e.g., Newman and Nash 2005). The correlation coefficient between the timing of the WPVs and eddy heat flux anomalies is 0.79 for all the WPV cases and 0.64 when the 2002 and 2019 SSWs are removed, both of which are statistically significant. This relationship is mainly contributed by the period from day −10 to day 0 (not shown), suggesting the dominant contribution from intense Rossby wave pulses shown in Fig. 6a. This result confirms the previous inference that more intense Rossby wave forcing is required for the early than the late WPVs to disturb the polar vortex and trigger the occurrence of the WPVs. The 2002 and 2019 Antarctic SSWs both occur in early September and are attributed to Rossby wave trains induced by tropical convection (Nishii and Nakamura 2004; Shen et al. 2020b). This implies that tropical convection is a potential candidate to alter the seasonality of the tropospheric wave activity and Antarctic WPVs.

In addition to the Rossby wave forcing, the state of the stratosphere itself can also influence the occurrence of the WPVs by modulating the propagation of the planetary-scale Rossby waves. It includes several aspects, such as the stratospheric equatorial wind (e.g., QBO; Holton and Tan 1980; Baldwin and Dunkerton 1998; Naito et al. 2003; Anstey and Shepherd 2014; Rao et al. 2021b) and the precondition of the stratospheric polar vortex (McIntyre 1982; Scaife et al. 2005). Figure 5a indicates a plausible linkage between the QBO and

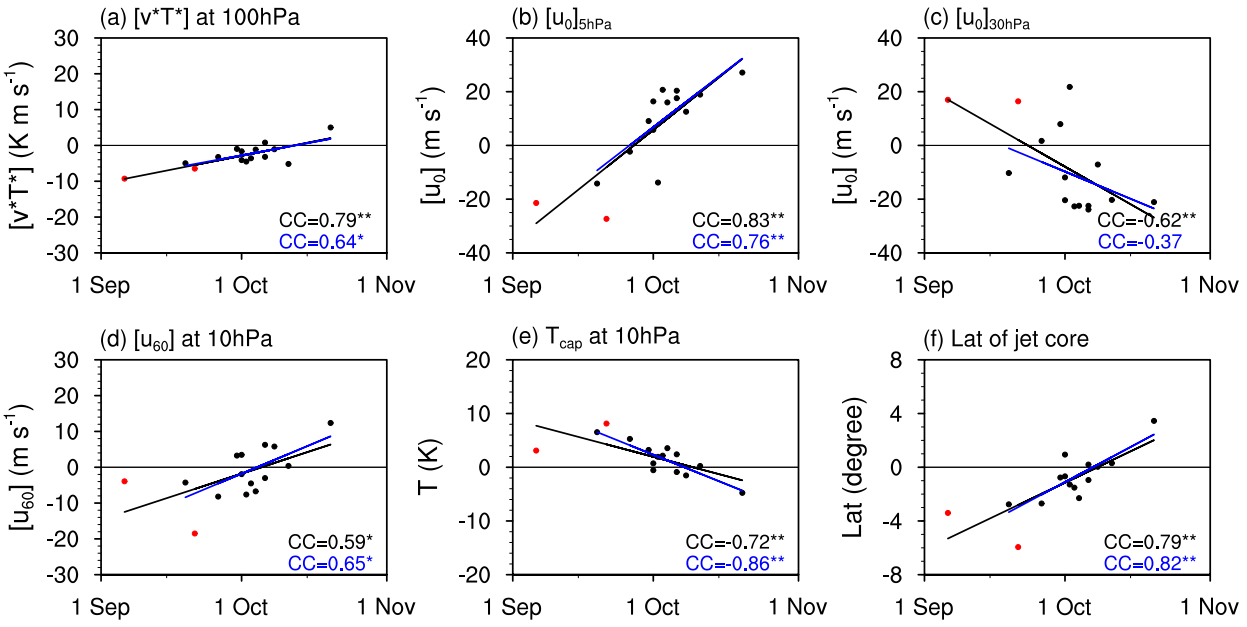

FIG. 9. (a) Scatter diagram between day 0 of Antarctic WPVs and the anomalies of eddy heat flux at 100 hPa averaged over 45°–75°S from day −40 to day 0. (b)–(f) As in (a), but the eddy heat flux is replaced by (b) $[u_0]_{5hPa}$, (c) $[u_0]_{30hPa}$, (d) $[u_{60}]$ at 10 hPa, (e) T_{cap} at 10 hPa, and (f) latitude of the circumpolar jet core at 10 hPa. Black lines are regression lines estimated from the least squares method using all WPVs. Blue lines are the same but exclude the 2002 and 2019 SSWs that are marked by red dots. CC indicates the correlation coefficient between x and y variables. One and two asterisks indicate the CC exceeds the 95% and 99% confidence levels based on the two-tailed Student's t test, respectively.

the Antarctic WPVs, and this linkage is further analyzed by considering the timing of the WPVs. Figures 9b and 9c show the scatterplots of the WPV timing (x axis) versus the equatorial zonal-mean zonal wind anomalies at 5 hPa ($[u_0]_{5hPa}$) and 30 hPa ($[u_0]_{30hPa}$) averaged from day −40 to day 0 (y axis), respectively. The two pressure levels are selected according to the centers of the zonal wind anomalies in Fig. 5a (Anstey and Shepherd 2014; Rao et al. 2020a). The correlation coefficient between the x and y variables exceeds the 99% confidence level for 5 and 30 hPa. It suggests that the QBO-like stratospheric equatorial wind may modulate the timing of WPVs. An easterly anomaly at the middle and upper equatorial stratosphere (e.g., 5 hPa) can induce a sharp zonal wind shear at the edge of the stratospheric polar vortex. This configuration leads to a steep potential vorticity gradient in the subtropics and changes the location of the critical surface (e.g., Holton and Tan 1980; Baldwin et al. 2001; Garfinkel et al. 2012; Rao et al. 2020b), setting a favorable background condition that hinders the propagation of planetary-scale Rossby waves toward the equator in the stratosphere (Gray et al. 2005). As a result, more Rossby waves tend to propagate poleward and disturb the polar vortex, contributing to the early occurrence of Antarctic WPVs. In contrast, an equatorial westerly anomaly at the middle and upper stratosphere leads to an opposite situation and late Antarctic WPVs. This result indicates a Holton–Tan-like relationship for the Southern Hemisphere on the subseasonal time scale, which was noticed in September (Shen et al. 2020b). The contrasting behavior of this relationship between September and October (Figs. 9b,c) may explain the invisibility of the seasonal-mean Holton–Tan relationship in the Southern Hemisphere (Hitchman and Huesmann 2009).

It is noteworthy that the above results do not mean that the easterly phase of upper stratospheric equatorial wind directly triggers the earlier occurrence of WPVs (Scaife et al. 2005; Shen et al. 2020b; Lim et al. 2021). In contrast, a favorable circulation condition is needed if a WPV event tends to occur in early spring, and the easterly phase of this QBO-like configuration provides such a favorable condition by altering the propagation of planetary waves (Gray et al. 2005). On the contrary, the seasonal cycle of the Antarctic polar vortex itself favors the occurrence of WPVs in late spring (Fig. 1; Baldwin et al. 2003). Thus, the role of upper stratospheric equatorial winds is insignificant in these late occurring cases.

The stratospheric circulation in the polar and subpolar region prior to the WPV is essential in setting the favorable precondition for the occurrence of the WPV (McIntyre 1982). For example, prolonged preconditioning was observed to precede the *major* Antarctic SSW in 2002 (Scaife et al. 2005) and the *minor* Antarctic SSW in 2019 (Lim et al. 2021). Here, three indices are defined to delineate the stratospheric precondition and its linkage to the Antarctic WPV timing. The first two indices reflect the intensity of the stratospheric polar vortex prior to the WPV, and they are defined as the $[u_{60}]$ anomalies at 10 hPa and T_{cap} anomalies at 10 hPa averaged from day −40 to day 0. The third index reflects the location of the polar night jet, and it is defined as the latitude of the maximum westerly at 10 hPa averaged from day −40 to day 0. The

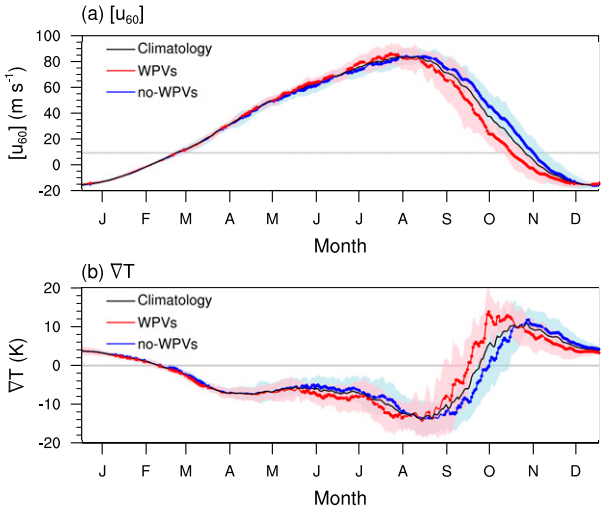

FIG. 10. Composited daily evolution of (a) $[u_{60}]$ and (b) ∇T at 10 hPa. Black, red, and blue lines indicate the climatology, years with Antarctic WPV, and years without Antarctic WPV, respectively. Thick red and blue dots indicate the difference between red and blue lines exceeds the 5th or 95th percentile estimated from 1000 bootstrapped samples. Red and blue shading refer to the corresponding boundary of one standard deviation.

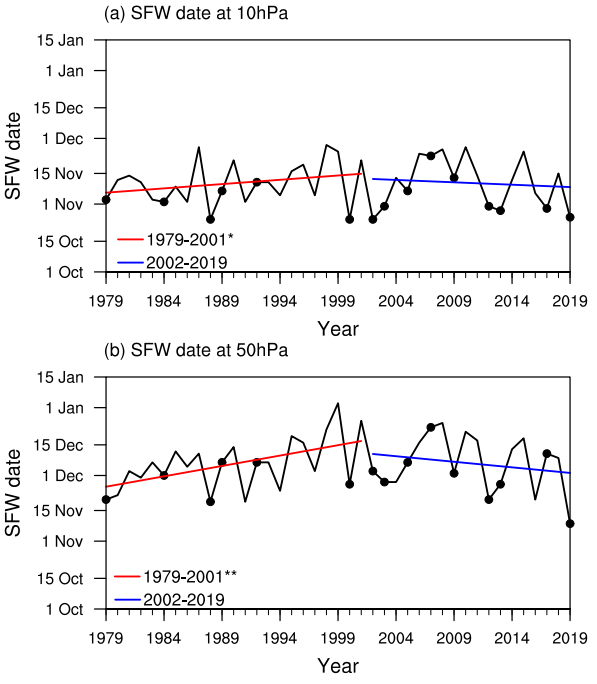

FIG. 11. (a) Timing of the SFW in the Southern Hemisphere (black line) for the period 1979–2019 based on SFWs defined at 10 hPa and its linear trends during 1979–2001 (red line) and 2002–19 (blue line), respectively. (b) As in (a), but for SFWs defined at 50 hPa. Black dots indicate years with WPVs. One and two asterisks indicate that the linear trend is significant at the 90% and 99% confidence level based on the two-tailed Student's *t* test, respectively.

scatterplots of the WPV timing versus the three indices suggest that a prior weakening (Figs. 9d,e) and contraction (Fig. 9f) of the Antarctic stratospheric polar vortex facilitates the early occurrence of the Antarctic WPV. This relationship remains significant and robust if the 2002 and 2019 SSWs are excluded (Figs. 9d–f). In addition, the plausible linkage between the Antarctic WPV's intensity and timing is also examined, and no clear relationship is found (not shown).

5. Impacts of the Antarctic WPVs

a. Impacts on the stratosphere

Previous studies suggest that the weakening or intensification of the stratospheric polar vortex may change the seasonal march in the stratosphere (Shiotani et al. 1993; Byrne and Shepherd 2018; Lim et al. 2018; Jucker et al. 2021). It motivates a similar comparison between years with and without WPVs to reveal the possible role of WPVs in altering the stratospheric seasonal cycle. Figure 10 shows the composited day-to-day evolution of $[u_{60}]$ and ∇T at 10 hPa. Climatologically, the date for $[u_{60}]$ at 10 hPa to fall below 10 m s^{-1} is 9 November, and the date for ∇T at 10 hPa to reverse is 8 October. The two dates both advance by approximately one week during years with WPVs, and they delay by approximately one week during years without WPVs. The differences in the seasonal transition between the two groups of years are half a month and significant at the 95% confidence level. In addition, the standard deviation of both $[u_{60}]$ and ∇T are smaller in years with WPVs than in years without WPVs during the seasonal transition. This result suggests that the occurrence of WPVs is associated with an earlier seasonal transition of the Antarctic stratospheric polar vortex, which is opposite to the effect of SSWs in the Northern Hemisphere (Hu et al. 2014).

The above analysis reveals a statistical relationship between the WPVs and seasonal transition. Considering that the SFW is also an indicator of the seasonal transition of the stratospheric polar vortex, the variability of the SFW is also investigated to understand further the interannual and interdecadal variation of the seasonal transition. Figure 2 suggests that there have been more Antarctic WPVs in the twenty-first century so far. Hence, it is inferred that the date of the SFW occurrence should advance after the year 2000. Figure 11 presents the interannual variation of the SFW date during 1979–2019. There is a significant trend of delayed occurrence of the SFW during 1979–2001 (Fig. 11, red line), in agreement with previous results (Waugh et al. 1999; Black and McDaniel 2007) and the strengthening trend of the Southern Hemisphere stratospheric polar vortex (Thompson and Solomon 2002). In contrast, an opposite trend appears after 2001 with a low confidence level, indicating an advance in the SFW date during the recent two decades (Fig. 11, blue line; Hirano et al. 2016; Rao and Garfinkel 2021). This recent weak trend indicates that the advanced SFW is likely caused by the large interannual variability associated with the frequent occurrence of WPVs (Fig. 11, black dots) rather than a long-term trend. The result remains almost the same if the 50-hPa level

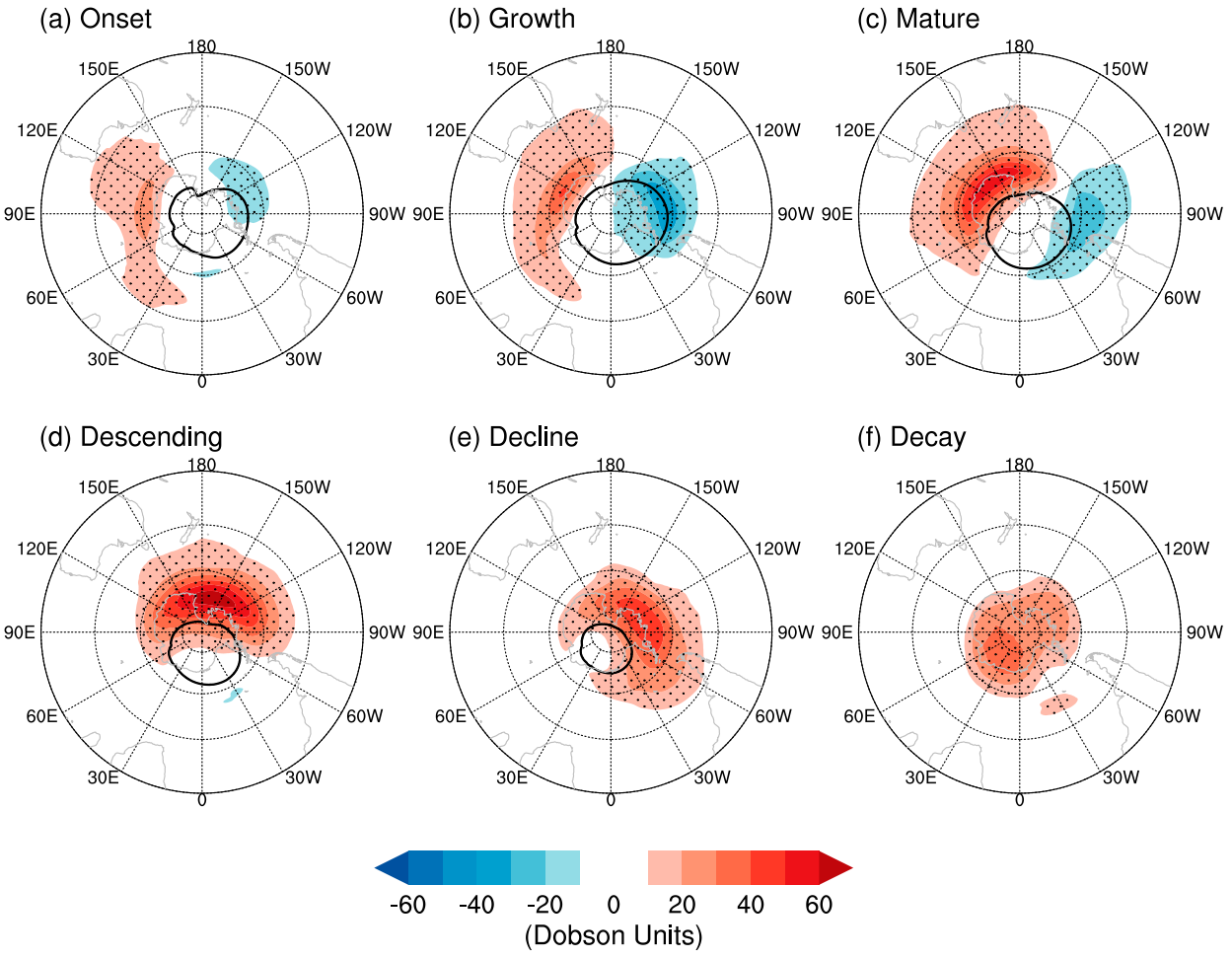

FIG. 12. Anomalies of total column ozone [shading; SI = 10 Dobson units (DU)] during different stages of the composite life cycle of Antarctic WPVs as in Fig. 4. Contour indicates the ozone hole, denoted as areas whose total column ozone is less than 220 DU. Black dots indicate ozone anomalies exceeding the 95% confidence level based on the two-tailed Student's *t* test. The total column ozone data are averaged from the MERRA-2 hourly data.

is used to define the SFW, and it further confirms the linkage between the WPVs and the accelerated seasonal cycle of the stratospheric polar vortex. Previous studies linked the early occurrence of the SFW to the rapid weakening of the stratospheric polar vortex (Lim et al. 2018, 2019), but the origin of the rapid weakening itself has not been understood well. Our results suggest that the early occurrence of the SFW can be partly attributed to the occurrence of the WPVs, which provides another perspective into understanding the variation of the SFWs. It should be kept in mind that the weakening of the stratospheric polar vortex associated with the early SFW may set a favorable stratospheric condition for the upward-propagating waves, which allows the occurrence of WPVs. Therefore, the causal relationship between WPVs and early SFW is complex. It cannot be distinguished solely based on the current analysis and deserves further study.

A conspicuous stratospheric influence of the Antarctic WPVs is on the polar-cap ozone concentration (Kanzawa and Kawaguchi 1990; Allen et al. 2003; Safieddine et al. 2020). On the one hand, high temperature during the WPVs suppresses the formation of the polar stratospheric clouds that facilitate ozone depletion (Solomon et al. 1986). On the other hand, the disturbed polar vortex during the WPVs facilitates meridional mixing between the ozone-poor polar-cap air and the ozone-rich midlatitude air (Newman 1986, 2010). Both the chemical and dynamical effects are conducive to increased polar ozone concentration during the WPVs. Figure 12 shows the composite of total column ozone anomalies during different stages of the WPV. During the onset stage, a prominent ozone-rich anomaly emerges in the Eastern Hemisphere and forms a dipole pattern together with an ozone-poor anomaly in the Western Hemisphere (Fig. 12a). This pattern intensifies from the growth to mature stages (Figs. 12b,c) and becomes a monopole ozone-rich center over the Antarctic during the descending to decay stages (Figs. 12d–f). The above anomalies resemble the geopotential height and temperature fields (Fig. 4), underlining the high consistency between ozone concentration and circulation (Seviour et al. 2014). The ozone-rich anomaly dominates in

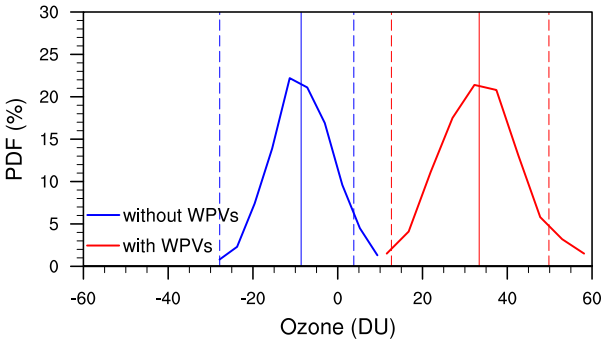

FIG. 13. PDF (solid curve) and median (vertical solid line) of the polar-cap ozone anomalies from day 0 to day +30 of the ∇T reversal estimates from 1000 bootstrapped samples in years with (red) and without (blue) Antarctic WPVs. The vertical dashed lines indicate the 5th and 95th percentiles. The polar-cap ozone data are from the NASA Ozone Watch.

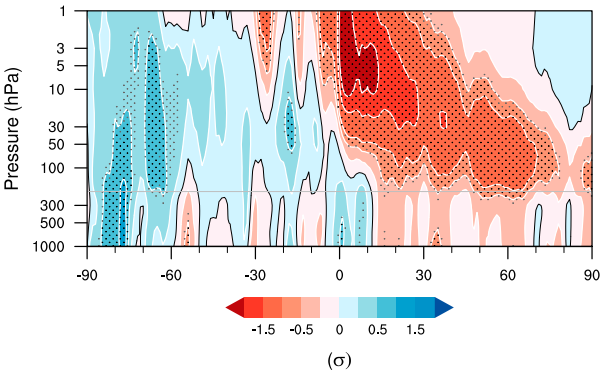

FIG. 14. Time–height development of the normalized daily SAM index (shading with contour; ±0.25, ±0.5, ±0.75, ±1.5, ±2.0; σ) during the composite life cycle of Antarctic WPVs. Thick black contours indicate zero values. The gray horizontal line indicates the approximate boundary between the troposphere and the stratosphere. Black and gray dots indicate values that exceed the 95% and 90% confidence level based on the two-tailed Student's *t* test, respectively.

this process. Therefore, the total column ozone is above average over the Antarctic during the life cycle of the WPV.

To further reveal the effects of the WPVs on ozone, the PDF of the polar-cap (south of 63°S) ozone anomalies from day 0 to day +30 is estimated with the bootstrap technique with 1000 resampling. The PDF is compared with that of the other ∇T reversal events that do not meet the criteria of WPVs, which can be regarded as regular seasonal cycles because ∇T reverses every year. The two PDFs are separated well from each other (Fig. 13). Moreover, the positive anomaly following WPVs is significantly different from zero at the 95% confidence level as estimated using the percentile method. This result confirms that Antarctic WPVs are associated with more pole-cap ozone and a smaller Antarctic ozone hole than periods with no WPVs.

b. Impacts on the troposphere

Figure 14 shows the time–height plot of the composite SAM index during WPVs. Weak negative SAM is observed surrounding day −25 in the middle to the upper stratosphere, consistent with the preconditioned stratospheric polar vortex. After day 0, the negative SAM amplifies in the upper stratosphere and gradually descends to the lower stratosphere during the three months following day 0. In this process, the tropospheric SAM index is mostly negative from day +10 to day +90, although it is weaker than its stratospheric counterpart, with the most significant signals trapped in the upper troposphere. This result agrees with Figs. 3c–e and some case studies (e.g., Shen et al. 2020b) and implies a possible influence of the Antarctic WPVs on the tropospheric climate. The less statistically significant SAM signal in the lower troposphere after day 0 is in accordance with the characteristics of eddy momentum flux anomalies in the troposphere (Figs. 6d–f). On the one hand, it may be due to the rareness of *major* SSW in the Southern Hemisphere discussed in section 3. On the other hand, it is also related to the diverse characteristics, such as the timing, duration, and amplitude, of the descending stratospheric signal following the Antarctic WPVs. This diversity may be related to the difference in the stratospheric conditions or the tropospheric process (Runde et al. 2016; Lim et al. 2020) that warrants further analysis.

Figure 15 shows the composite anomalies of sea level pressure, surface air temperature, and precipitation averaged from day 0 to day +90 of the Antarctic WPVs. Significant high and low sea level pressure anomalies are located over the Antarctic and the surrounding high latitudes, respectively, especially to the southeast of South America (Fig. 15a). It resembles the negative phase of the SAM to some extent and is consistent with Fig. 14. Accordingly, significant warming is observed over most of Antarctica, southern and eastern Australia, and central South America, and significant cooling is observed over the South Atlantic and the subpolar region southward of 30°S (Fig. 15b). The distribution of temperature anomalies can be explained well by the temperature advection associated with the SAM-like pattern (Fig. 15a). The precipitation also shows large-scale responses to the Antarctic WPVs, although its signals are less organized and statistically significant than the temperature (Figs. 15b,c). For example, enhanced precipitation is observed over the western coast of the Ross Sea, the Antarctic Peninsula, southern South America, and Madagascar (Fig. 15c). Reduced precipitation is observed over the western Antarctic, eastern Australia, South Africa, and the eastern part of subtropical South America. Especially, the reduced precipitation over eastern Australia is robust (not shown). Together with the warm anomalies, it sets a favorable condition for wildfires, which was seen in 2019 (Lim et al. 2019, 2021; Shen et al. 2020b). These results underscore the potential role of WPVs in improving seasonal climate prediction in the Southern Hemisphere and wildfire risk warnings in Australia (Bett et al. 2020).

6. Summary

This study proposes criteria to identify Antarctic WPVs and investigates their occurrence, variability, composite life cycle,

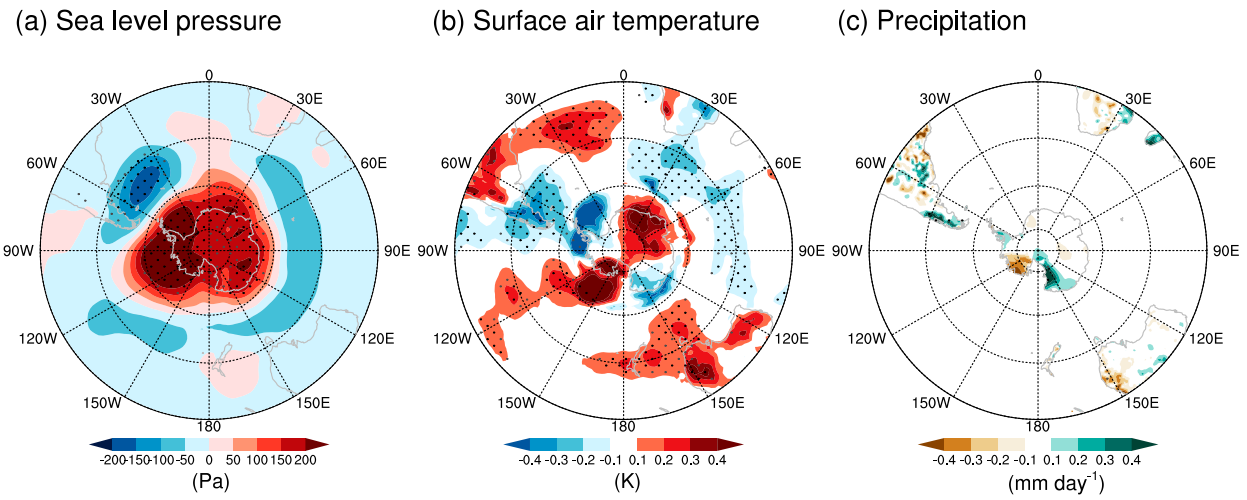

FIG. 15. Composite anomalies of (a) sea level pressure (SI = 50 hPa), (b) surface air temperature (SI = 0.1 K), and (c) precipitation (SI = 0.1 mm day^{-1}) averaged between day 0 and day +90. Black and gray dots indicate values exceeding the 95% and 90% confidence level based on the two-tailed Student's *t* test, respectively.

and impacts. The criteria are based on the pole-to-midlatitude temperature gradient reversal in the stratosphere. Hence, the analysis reflects the stratospheric polar vortex variability that resembles the SSWs, although only one *major* SSW has been observed. The Antarctic stratospheric polar vortex is stronger and more stable than the Arctic one. Hence, Antarctic WPVs are mostly observed in austral spring (September and October) when the stratospheric polar vortex becomes weak, and they require more wave forcing the earlier they occur in the season. Its mean frequency is approximately 0.4 events per year and is lower than the Northern Hemispheric *major* SSWs (Charlton and Polvani 2007; Baldwin et al. 2021).

Enhanced upward-propagating Rossby waves explain the occurrence and dynamics of Antarctic WPVs. Strong eddy heat flux anomalies are observed before the mature stage of the WPVs, and they are mainly contributed by wavenumber 1, which is evident in both the troposphere and the stratosphere. It is followed by strong deceleration of the polar night jet and warming of the polar stratosphere, both of which descend with time. When the zonal wind anomalies reach the lower stratosphere, strong equatorward eddy momentum fluxes appear in the upper troposphere and contribute to the tropospheric responses to the WPVs. This process is dominated by wavenumbers 3 and higher, although all wavenumbers contribute. The timing of the Antarctic WPVs varies on the subseasonal time scale and is associated with the stratospheric preconditions. The early occurrence of the Antarctic WPVs is preceded by both a weakened and contracted Antarctic stratospheric polar vortex and a QBO-like equatorial easterly anomaly in the middle and upper stratosphere.

Antarctic WPVs facilitate the increase of the total column ozone over the Antarctic on both a subseasonal and interannual time scale. It is also closely related to the advanced seasonal transition of the stratospheric polar vortex. The frequency of the Antarctic WPVs is low before the year 2000 and doubles after that. This change is associated with the advanced SFW after the year 2000. The Antarctic WPVs are accompanied by significant negative SAM signals in the upper stratosphere, which further descend into the lower stratosphere and troposphere in approximately three months. Although this descending process is somewhat noisy and varies among different cases, it is more persistent than its counterpart in Northern Hemisphere (Baldwin and Dunkerton 2001; Thompson et al. 2005) and can lead to hemispheric responses in surface air temperature and precipitation. The persistent tropospheric response is possibly related to the long life cycle of the Antarctic WPVs. The circumpolar westerly jet weakens and persists for one month (Fig. 3a), setting a favorable circulation condition for upward propagation of planetary waves until the descending phase (Figs. 5b and 6a). Accordingly, the weakening of the stratospheric polar vortex persists, leading to a prolonged negative SAM signal in the troposphere.

Acknowledgments. We thank the three anonymous reviewers for their insightful comments and suggestions that helped us improve the paper's quality significantly. The work of XS and LW was supported by the National Natural Science Foundation of China (41925020 and 41721004) and the Chinese Academy of Sciences (QYZDY-SSW-DQC024). The work of SO was supported by the National Centre for Atmospheric Science (NCAS) of the Natural Environment Research Council (NERC), the NERC North Atlantic Climate System Integrated Study (ACSIS) (NE/N018001), and the Belmont-Forum GOTHAM project (NE/P006779/1). The work of SCH and AAS was supported by the U.K.–China Research and Innovation Partnership Fund through the Met Office Climate Science for Service Partnership (CSSP) China as part of the Newton Fund.

Data availability statement. The JRA-55 reanalysis data were downloaded from https://jra.kishou.go.jp/JRA-55/index_

en.html. The ERA5 and ERA-Interim reanalysis data were downloaded from https://www.ecmwf.int/en/forecasts/datasets/browse-reanalysis-datasets. The NCEP–NCAR reanalysis data were downloaded from https://psl.noaa.gov/data/gridded/data.ncep.reanalysis.html. The MERRA-2 reanalysis data were obtained from https://gmao.gsfc.nasa.gov/reanalysis/MERRA-2. The daily polar-cap ozone data from NASA ozone watch were downloaded from https://ozonewatch.gsfc.nasa.gov. CPC Global Unified Precipitation data were downloaded from https://psl.noaa.gov/data/gridded/data.cpc.globalprecip.html.

REFERENCES

Allen, D. R., R. M. Bevilacqua, G. E. Nedoluha, C. E. Randall, and G. L. Manney, 2003: Unusual stratospheric transport and mixing during the 2002 Antarctic winter. *Geophys. Res. Lett.*, **30**, 1599, https://doi.org/10.1029/2003GL017117.

Andrews, D. G., J. R. Holton, and C. B. Leovy, 1987: *Middle Atmosphere Dynamics*. Academic Press, 489 pp.

Anstey, J. A., and T. G. Shepherd, 2014: High-latitude influence of the quasi-biennial oscillation. *Quart. J. Roy. Meteor. Soc.*, **140** (678), 1–21, https://doi.org/10.1002/qj.2132.

Baldwin, M. P., and T. J. Dunkerton, 1998: Quasi-biennial modulation of the Southern Hemisphere stratospheric polar vortex. *Geophys. Res. Lett.*, **25**, 3343–3346, https://doi.org/10.1029/98GL02445.

——, and ——, 1999: Propagation of the Arctic Oscillation from the stratosphere to the troposphere. *J. Geophys. Res.*, **104**, 30 937–30 946, https://doi.org/10.1029/1999JD900445.

——, and ——, 2001: Stratospheric harbingers of anomalous weather regimes. *Science*, **294**, 581–584, https://doi.org/10.1126/science.1063315.

——, and Coauthors, 2001: The quasi-biennial oscillation. *Rev. Geophys.*, **39**, 179–229, https://doi.org/10.1029/1999RG000073.

——, D. B. Stephenson, D. W. J. Thompson, T. J. Dunkerton, A. J. Charlton, and A. O'Neill, 2003: Stratospheric memory and skill of extended-range weather forecasts. *Science*, **301**, 636–640, https://doi.org/10.1126/science.1087143.

——, and Coauthors, 2021: Sudden stratospheric warmings. *Rev. Geophys.*, **59**, e2020RG000708, https://doi.org/10.1029/2020RG000708.

Bett, P. E., K. E. Williams, C. Burton, A. A. Scaife, A. J. Wiltshire, and R. Gilham, 2020: Skillful seasonal prediction of key carbon cycle components: NPP and fire risk. *Environ. Res. Commun.*, **2**, 055002, https://doi.org/10.1088/2515-7620/ab8b29.

Black, R. X., and B. A. McDaniel, 2007: Interannual variability in the Southern Hemisphere circulation organized by stratospheric final warming events. *J. Atmos. Sci.*, **64**, 2968–2974, https://doi.org/10.1175/JAS3979.1.

Butler, A. H., D. J. Seidel, S. C. Hardiman, N. Butchart, T. Birner, and A. Match, 2015: Defining sudden stratospheric warmings. *Bull. Amer. Meteor. Soc.*, **96**, 1913–1928, https://doi.org/10.1175/BAMS-D-13-00173.1.

Byrne, N. J., and T. G. Shepherd, 2018: Seasonal persistence of circulation anomalies in the Southern Hemisphere stratosphere and its implications for the troposphere. *J. Climate*, **31**, 3467–3483, https://doi.org/10.1175/JCLI-D-17-0557.1.

Charlton, A. J., and L. M. Polvani, 2007: A new look at stratospheric sudden warmings. Part I: Climatology and modeling benchmarks. *J. Climate*, **20**, 449–469, https://doi.org/10.1175/JCLI3996.1.

——, A. O'Neill, W. A. Lahoz, and P. Berrisford, 2005: The splitting of the stratospheric polar vortex in the Southern Hemisphere, September 2002: Dynamical evolution. *J. Atmos. Sci.*, **62**, 590–602, https://doi.org/10.1175/JAS-3318.1.

Charney, J. G., and P. G. Drazin, 1961: Propagation of planetary-scale disturbances from lower into upper atmosphere. *J. Geophys. Res.*, **66**, 83–109, https://doi.org/10.1029/JZ066i001p00083.

Chen, M., W. Shi, P. Xie, V. B. S. Silva, V. E. Kousky, R. W. Higgins, and J. E. Janowiak, 2008: Assessing objective techniques for gauge-based analyses of global daily precipitation. *J. Geophys. Res.*, **113**, D04110, https://doi.org/10.1029/2007JD009132.

Dee, D. P., and Coauthors, 2011: The ERA-Interim reanalysis: Configuration and performance of the data assimilation system. *Quart. J. Roy. Meteor. Soc.*, **137**, 553–597, https://doi.org/10.1002/qj.828.

Domeisen, D. I., 2019: Estimating the frequency of sudden stratospheric warming events from surface observations of the North Atlantic Oscillation. *J. Geophys. Res. Atmos.*, **124**, 3180–3194, https://doi.org/10.1029/2018JD030077.

——, and Coauthors, 2020: The role of the stratosphere in subseasonal to seasonal prediction: 2. Predictability arising from stratosphere–troposphere coupling. *J. Geophys. Res. Atmos.*, **125**, e2019JD030923, https://doi.org/10.1029/2019JD030923.

Efron, B., and R. J. Tibshirani, 1994: *An Introduction to the Bootstrap*. Chapman and Hall, 456 pp.

Eswaraiah, S., Y. H. Kim, H. Liu, M. V. Ratnam, and J. Lee, 2017: Do minor sudden stratospheric warmings in the Southern Hemisphere (SH) impact coupling between stratosphere and mesosphere–lower thermosphere (MLT) like major warmings? *Earth Planets Space*, **69**, 119, https://doi.org/10.1186/s40623-017-0704-5.

Garfinkel, C. I., T. A. Shaw, D. L. Hartmann, and D. W. Waugh, 2012: Does the Holton–Tan mechanism explain how the quasi-biennial oscillation modulates the Arctic polar vortex? *J. Atmos. Sci.*, **69**, 1713–1733, https://doi.org/10.1175/JAS-D-11-0209.1.

——, L. D. Oman, E. A. Barnes, D. W. Waugh, M. H. Hurwitz, and A. M. Molod, 2013: Connections between the spring breakup of the Southern Hemisphere polar vortex, stationary waves, and air–sea roughness. *J. Atmos. Sci.*, **70**, 2137–2151, https://doi.org/10.1175/JAS-D-12-0242.1.

Gelaro, R., and Coauthors, 2017: The Modern-Era Retrospective Analysis for Research and Applications, version 2 (MERRA-2). *J. Climate*, **30**, 5419–5454, https://doi.org/10.1175/JCLI-D-16-0758.1.

Goyal, R., M. Jucker, A. S. Gupta, H. H. Hendon, and M. H. England, 2021: Zonal wave 3 pattern in the Southern Hemisphere generated by tropical convection. *Nat. Geosci.*, **14**, 732–738, https://doi.org/10.1038/s41561-021-00811-3.

Gray, L., W. Norton, C. Pascoe, and A. Charlton, 2005: A possible influence of equatorial winds on the September 2002 Southern Hemisphere sudden warming event. *J. Atmos. Sci.*, **62**, 651–667, https://doi.org/10.1175/JAS-3339.1.

Hardiman, S. C., and Coauthors, 2011: Improved predictability of the troposphere using stratospheric final warmings. *J. Geophys. Res.*, **116**, D18113, https://doi.org/10.1029/2011JD015914.

Hersbach, H., and Coauthors, 2020: The ERA5 global reanalysis. *Quart. J. Roy. Meteor. Soc.*, **146**, 1999–2049, https://doi.org/10.1002/qj.3803.

Hio, Y., and S. Yoden, 2005: Interannual variations of the seasonal march in the Southern Hemisphere stratosphere for 1979–2002 and characterization of the unprecedented year

2002. *J. Atmos. Sci.*, **62**, 567–580, https://doi.org/10.1175/JAS-3333.1.

Hirano, S., M. Kohma, and K. Sato, 2016: A three-dimensional analysis on the role of atmospheric waves in the climatology and interannual variability of stratospheric final warming in the Southern Hemisphere. *J. Geophys. Res. Atmos.*, **121**, 8429–8443, https://doi.org/10.1002/2015JD024481.

Hirota, I., K. Kuroi, and M. Shiotani, 1990: Midwinter warmings in the Southern Hemisphere stratosphere in 1988. *Quart. J. Roy. Meteor. Soc.*, **116**, 929–941, https://doi.org/10.1002/qj.49711649407.

Hitchman, M. H., and A. S. Huesmann, 2009: Seasonal influence of the quasi-biennial oscillation on stratospheric jets and Rossby wave breaking. *J. Atmos. Sci.*, **66**, 935–946, https://doi.org/10.1175/2008JAS2631.1.

Holton, J. R., and H. C. Tan, 1980: The influence of the equatorial quasi-biennial oscillation on the global circulation at 50 mb. *J. Atmos. Sci.*, **37**, 2200–2208, https://doi.org/10.1175/1520-0469(1980)037<2200:TIOTEQ>2.0.CO;2.

Horan, M. F., and T. Reichler, 2017: Modeling seasonal sudden stratospheric warming climatology based on polar vortex statistics. *J. Climate*, **30**, 10 101–10 116, https://doi.org/10.1175/JCLI-D-17-0257.1.

Hu, J. G., R. C. Ren, and H. M. Xu, 2014: Occurrence of winter stratospheric sudden warming events and the seasonal timing of spring stratospheric final warming. *J. Atmos. Sci.*, **71**, 2319–2334, https://doi.org/10.1175/JAS-D-13-0349.1.

Hu, Y., and Q. Fu, 2009: Stratospheric warming in Southern Hemisphere high latitudes since 1979. *Atmos. Chem. Phys.*, **9**, 4329–4340, https://doi.org/10.5194/acp-9-4329-2009.

Jucker, M., 2016: Are sudden stratospheric warmings generic? Insights from an idealized GCM. *J. Atmos. Sci.*, **73**, 5061–5080, https://doi.org/10.1175/JAS-D-15-0353.1.

——, S. Fueglistaler, and G. K. Vallis, 2014: Stratospheric sudden warmings in an idealized GCM. *J. Geophys. Res. Atmos.*, **119**, 11 054–11 064, https://doi.org/10.1002/2014JD022170.

——, T. Reichler, and D. W. Waugh, 2021: How frequent are Antarctic sudden stratospheric warmings in present and future climate? *Geophys. Res. Lett.*, **48**, e2021GL093215, https://doi.org/10.1029/2021GL093215.

Kalnay, E., and Coauthors, 1996: The NCEP/NCAR 40-Year Reanalysis Project. *Bull. Amer. Meteor. Soc.*, **77**, 437–471, https://doi.org/10.1175/1520-0477(1996)077<0437:TNYRP>2.0.CO;2.

Kanzawa, H., and S. Kawaguchi, 1990: Large stratospheric sudden warming in Antarctic late winter and shallow ozone hole in 1988. *Geophys. Res. Lett.*, **17**, 77–80, https://doi.org/10.1029/GL017i001p00077.

Kidston, J., A. A. Scaife, S. C. Hardiman, D. M. Mitchell, N. Butchart, M. P. Baldwin, and L. J. Gray, 2015: Stratospheric influence on tropospheric jet streams, storm tracks and surface weather. *Nat. Geosci.*, **8**, 433–440, https://doi.org/10.1038/ngeo2424.

Kobayashi, S., and Coauthors, 2015: The JRA-55 reanalysis: General specifications and basic characteristics. *J. Meteor. Soc. Japan*, **93**, 5–48, https://doi.org/10.2151/jmsj.2015-001.

Kolstad, E. W., T. Breiteig, and A. A. Scaife, 2010: The association between stratospheric weak polar vortex events and cold air outbreaks in the Northern Hemisphere. *Quart. J. Roy. Meteor. Soc.*, **136**, 886–893, https://doi.org/10.1002/qj.620.

Kwon, H., H. Choi, B.-M. Kim, S.-W. Kim, and S.-J. Kim, 2020: Recent weakening of the southern stratospheric polar vortex and its impact on the surface climate over Antarctica. *Environ. Res. Lett.*, **15**, 094072, https://doi.org/10.1088/1748-9326/ab9d3d.

Lim, E. P., H. H. Hendon, and D. W. J. Thompson, 2018: Seasonal evolution of stratosphere–troposphere coupling in the Southern Hemisphere and implications for the predictability of surface climate. *J. Geophys. Res. Atmos.*, **123**, 12 002–12 016, https://doi.org/10.1029/2018JD029321.

——, ——, G. Boschat, D. Hudson, D. W. J. Thompson, A. J. Dowdy, and J. M. Arblaster, 2019: Australian hot and dry extremes induced by weakenings of the stratospheric polar vortex. *Nat. Geosci.*, **12**, 896–901, https://doi.org/10.1038/s41561-019-0456-x.

——, and Coauthors, 2020: The 2019 Antarctic sudden stratospheric warming. *SPARC Newsletter*, No. 54, SPARC International Project Office, Oberpfaffenhofen, Germany, 10–13, www.sparc-climate.org/wp-content/uploads/sites/5/2017/12/SPARCnewsletter_Jan2020_WEB.pdf.

——, and Coauthors, 2021: The 2019 Southern Hemisphere stratospheric polar vortex weakening and its impacts. *Bull. Amer. Meteor. Soc.*, **102**, E1150–E1171, https://doi.org/10.1175/BAMS-D-20-0112.1.

Limpasuvan, V., D. W. J. Thompson, and D. L. Hartmann, 2004: The life cycle of the Northern Hemisphere sudden stratospheric warmings. *J. Climate*, **17**, 2584–2596, https://doi.org/10.1175/1520-0442(2004)017<2584:TLCOTN>2.0.CO;2.

Manney, G. L., and Coauthors, 2005: Simulations of dynamics and transport during the September 2002 Antarctic major warming. *J. Atmos. Sci.*, **62**, 690–707, https://doi.org/10.1175/JAS-3313.1.

Matsuno, T., 1971: Dynamical model of stratospheric sudden warming. *J. Atmos. Sci.*, **28**, 1479–1494, https://doi.org/10.1175/1520-0469(1971)028<1479:ADMOTS>2.0.CO;2.

McIntyre, M. E., 1982: How well do we understand the dynamics of stratospheric warmings? *J. Meteor. Soc. Japan*, **60**, 37–65, https://doi.org/10.2151/jmsj1965.60.1_37.

Mechoso, C. R., A. O'Neill, V. D. Pope, and J. D. Farrara, 1988: A study of the stratospheric final warming of 1982 in the Southern Hemisphere. *Quart. J. Roy. Meteor. Soc.*, **114**, 1365–1384, https://doi.org/10.1002/qj.49711448402.

Naito, Y., M. Taguchi, and S. Yoden, 2003: A parameter sweep experiment on the effects of the equatorial QBO on stratospheric sudden warming events. *J. Atmos. Sci.*, **60**, 1380–1394, https://doi.org/10.1175/1520-0469(2003)060<1380:APSEOT>2.0.CO;2.

Newman, P. A., 1986: The final warming and polar vortex disappearance during the Southern Hemisphere spring. *Geophys. Res. Lett.*, **13**, 1228–1231, https://doi.org/10.1029/GL013i012p01228.

——, 2010: Chemistry and dynamics of the Antarctic ozone hole. *The Stratosphere: Dynamics, Transport, and Chemistry*, *Geophys. Monogr.*, Vol. 190, Amer. Geophys. Union, 157–171.

——, and E. R. Nash, 2005: The unusual Southern Hemisphere stratosphere winter of 2002. *J. Atmos. Sci.*, **62**, 614–628, https://doi.org/10.1175/JAS-3323.1.

Nishii, K., and H. Nakamura, 2004: Tropospheric influence on the diminished Antarctic ozone hole in September 2002. *Geophys. Res. Lett.*, **31**, L16103, https://doi.org/10.1029/2004GL019532.

Pedatella, N. M., and Coauthors, 2018: How sudden stratospheric warming affects the whole atmosphere. *Eos, Trans. Amer. Geophys. Union*, **99**, https://doi.org/10.1029/2018EO092441.

Plumb, R. A., 1989: On the seasonal cycle of stratospheric planetary waves. *Pure Appl. Geophys.*, **130**, 233–242, https://doi.org/10.1007/BF00874457.

Polvani, L. M., and D. W. Waugh, 2004: Upward wave activity flux as a precursor to extreme stratospheric events and subsequent anomalous surface weather regimes. *J. Climate*, **17**, 3548–3554, https://doi.org/10.1175/1520-0442(2004)017<3548:UWAFAA>2.0.CO;2.

Rao, J., and C. I. Garfinkel, 2021: Projected changes of stratospheric final warmings in the Northern and Southern Hemispheres by CMIP5/6 models. *Climate Dyn.*, **56**, 3353–3371, https://doi.org/10.1007/s00382-021-05647-6.

——, ——, I. P. White, and C. Schwartz, 2020a: The Southern Hemisphere minor sudden stratospheric warming in September 2019 and its predictions in S2S models. *J. Geophys. Res. Atmos.*, **125**, e2020JD032723, https://doi.org/10.1029/2020JD032723.

——, ——, and ——, 2020b: Impact of the quasi-biennial oscillation on the northern winter stratospheric polar vortex in CMIP5/6 models. *J. Climate*, **33**, 4787–4813, https://doi.org/10.1175/JCLI-D-19-0663.1.

——, S. Liu, and Y. Chen, 2021a: Northern Hemisphere sudden stratospheric warming and its downward impact in four Chinese CMIP6 models. *Adv. Atmos. Sci.*, **38**, 187–202, https://doi.org/10.1007/s00376-020-0250-0.

——, C. I. Garfinkel, and I. P. White, 2021b: Development of the extratropical response to the stratospheric quasi-biennial oscillation. *J. Climate*, **34**, 7239–7255, https://doi.org/10.1175/JCLI-D-20-0960.1.

Runde, T., M. Dameris, H. Garny, and D. E. Kinnison, 2016: Classification of stratospheric extreme events according to their downward propagation to the troposphere. *Geophys. Res. Lett.*, **43**, 6665–6672, https://doi.org/10.1002/2016GL069569.

Safieddine, S., and Coauthors, 2020: Antarctic ozone enhancement during the 2019 sudden stratospheric warming event. *Geophys. Res. Lett.*, **47**, e2020GL087810, https://doi.org/10.1029/2020GL087810.

Scaife, A. A., and I. N. James, 2000: Response of the stratosphere to interannual variability of tropospheric planetary waves. *Quart. J. Roy. Meteor. Soc.*, **126**, 275–297, https://doi.org/10.1002/qj.49712656214.

——, D. R. Jackson, R. Swinbank, N. Butchart, H. Thornton, M. Keil, and L. Henderson, 2005: Stratospheric vacillations and the major warming over Antarctica in 2002. *J. Atmos. Sci.*, **62**, 629–639, https://doi.org/10.1175/JAS-3334.1.

——, and Coauthors, 2016: Seasonal winter forecasts and the stratosphere. *Atmos. Sci. Lett.*, **17**, 51–56, https://doi.org/10.1002/asl.598.

Seviour, W. J. M., S. C. Hardiman, L. J. Gray, N. Butchart, C. MacLachlan, and A. A. Scaife, 2014: Skillful seasonal prediction of the southern annular mode and Antarctic ozone. *J. Climate*, **27**, 7462–7474, https://doi.org/10.1175/JCLI-D-14-00264.1.

Shaw, T. A., J. Perlwitz, N. Harnik, P. A. Newman, and S. Pawson, 2011: The impact of stratospheric ozone changes on downward wave coupling in the Southern Hemisphere. *J. Climate*, **24**, 4210–4229, https://doi.org/10.1175/2011JCLI4170.1.

Shen, X., L. Wang, and S. Osprey, 2020a: The Southern Hemisphere sudden stratospheric warming of September 2019. *Sci. Bull.*, **65**, 1800–1802, https://doi.org/10.1016/j.scib.2020.06.028.

——, ——, and ——, 2020b: Tropospheric forcing of the 2019 Antarctic sudden stratospheric warming. *Geophys. Res. Lett.*, **47,** e2020GL089343, https://doi.org/10.1029/2020GL089343.

Shiotani, M., N. Shimoda, and I. Hirota, 1993: Interannual variability of the stratospheric circulation in the Southern Hemisphere. *Quart. J. Roy. Meteor. Soc.*, **119**, 531–546, https://doi.org/10.1002/qj.49711951110.

Sjoberg, J. P., and T. Birner, 2012: Transient tropospheric forcing of sudden stratospheric warmings. *J. Atmos. Sci.*, **69**, 3420–3432, https://doi.org/10.1175/JAS-D-11-0195.1.

Solomon, S., R. R. Garcia, F. S. Rowland, and D. J. Wuebbles, 1986: On the depletion of Antarctic ozone. *Nature*, **321**, 755–758, https://doi.org/10.1038/321755a0.

——, D. J. Ivy, D. Kinnison, M. J. Mills, R. R. Neely, and A. Schmidt, 2016: Emergence of healing in the Antarctic ozone layer. *Science*, **353**, 269–274, https://doi.org/10.1126/science.aae0061.

Thompson, D. W. J., and S. Solomon, 2002: Interpretation of recent Southern Hemisphere climate change. *Science*, **296**, 895–899, https://doi.org/10.1126/science.1069270.

——, M. P. Baldwin, and S. Solomon, 2005: Stratosphere–troposphere coupling in the Southern Hemisphere. *J. Atmos. Sci.*, **62**, 708–715, https://doi.org/10.1175/JAS-3321.1.

Trenberth, K. E., and J. T. Fasullo, 2013: An apparent hiatus in global warming? *Earth's Future*, **1**, 19–32, https://doi.org/10.1002/2013EF000165.

Wang, L., S. C. Hardiman, P. E. Bett, R. E. Comer, C. Kent, and A. A. Scaife, 2020: What chance of a sudden stratospheric warming in the Southern Hemisphere? *Environ. Res. Lett.*, **15**, 104038, https://doi.org/10.1088/1748-9326/aba8c1.

Wargan, K., B. Weir, G. L. Manney, S. E. Cohn, and N. J. Livesey, 2020: The anomalous 2019 Antarctic ozone hole in the GEOS Constituent Data Assimilation System with MLS observations. *J. Geophys. Res. Atmos.*, **125**, e2020JD033335, https://doi.org/10.1029/2020JD033335.

Waugh, D. W., and W. J. Randel, 1999: Climatology of Arctic and Antarctic polar vortices using elliptical diagnostics. *J. Atmos. Sci.*, **56**, 1594–1613, https://doi.org/10.1175/1520-0469(1999)056<1594:COAAAP>2.0.CO;2.

——, and L. M. Polvani, 2010: Stratospheric polar vortices. *The Stratosphere: Dynamics, Transport, and Chemistry*, *Geophys. Monogr.*, Vol. 190, Amer. Geophys. Union, 43–57.

——, W. J. Randel, S. Pawson, P. A. Newman, and E. R. Nash, 1999: Persistence of the lower stratospheric polar vortices. *J. Geophys. Res.*, **104**, 27 191–27 201, https://doi.org/10.1029/1999JD900795.

White, I., C. I. Garfinkel, E. P. Gerber, M. Jucker, V. Aquila, and L. D. Oman, 2019: The downward influence of sudden stratospheric warmings: Association with tropospheric precursors. *J. Climate*, **32**, 85–108, https://doi.org/10.1175/JCLI-D-18-0053.1.

Xie, P., A. Yatagai, M. Chen, T. Hayasaka, Y. Fukushima, C. Liu, and S. Yang, 2007: A Gauge-based analysis of daily precipitation over East Asia. *J. Hydrometeor.*, **8**, 607–626, https://doi.org/10.1175/JHM583.1.

Yeh, S. W., J. S. Kug, B. Dewitte, M. H. Kwon, B. P. Kirtman, and F.-F. Jin, 2009: El Niño in a changing climate. *Nature*, **461**, 511–514, https://doi.org/10.1038/nature08316.